CALCULATION OF PARITY VIOLATING EFFECTS IN THE $6^2P_{\frac{1}{2}}$ $7^2P_{\frac{1}{2}}$ FORBIDDEN M1 TRANSITION IN THALLIUM

David V. Neuffer

and

Eugene D. Commins

Physics Department, University of California

Berkeley, California 94704

and

Materials and Molecular Research Division

Lawrence Berkeley Laboratory

Berkeley, California 94720

† Research supported by United States Energy Research and Development Administration.

* To be submitted to Physical Review A.

TABLE OF CONTENTS

Abstract v
Acknowledgments vii
I. CALCULATION OF PARITY VIOLATING EFFECTS IN THE $6^2P_{1/2}$-$7^2P_{1/2}$ FORBIDDEN M1 TRANSITION IN THALLIUM 2
1. Introduction 2
2. Thallium Wave Functions in the One-Electron Central Field Approximation. 6
2.1 Construction of wave functions 6
2.2 Hyperfine structure 9
2.3 Fine structure. 10
2.4 Allowed electric dipole transitions 11
3. Magnetic Dipole Transition Rates 13
3.1 The relativistic contribution 13
3.2 Interconfiguration interaction correction 15
3.3 Breit interaction corrections 18
3.4 Total theoretical M1 rate; corrections to $g_J(Tl,6^2P_{1/2})$. 21
3.5 Hyperfine mixing. 22
3.6 Other M1 transitions 23
4. Parity Violating E1 Amplitudes 24
4.1 $6^2P_{1/2}$-$7^2P_{1/2}$ transitions 24
4.2 Other parity-violating transitions. 27
5. Stark Effect 27
5.1 $6^2P_{1/2}$-$7^2P_{1/2}$ transitions 27
5.2 Experimental determination of M1 amplitude. 29
5.3 Interference of $\mathcal{E}_{PV}$ and $\mathcal{E}_S$. 30
6. Parity Violation in $^2P_{1/2}$-$^2P_{3/2}$ Transitions. 31
References 33
Figure Captions. 36
Appendix A 39
Appendix B 43
Appendix C 44

(CONTENTS, continued)

II. CALCULATIONS OF PARITY VIOLATION IN FORBIDDEN M1 TRANSITIONS IN CESIUM

1. Introduction 61

2. Cesium Wave Functions in the One-Electron Central Field Approximation 62

2.1 Construction of electronic wave-functions 62

2.2 Hyperfine splittings 63

2.3 Allowed E1 transition rates 63

3. Magnetic Dipole Transition Rates 66

4. Calculation of Parity Violating E1 Amplitude 72

5. Calculation of the Stark Effect E1 Transitions 76

References 81

CALCULATION OF PARITY VIOLATING EFFECTS IN THE $6^2P_{\frac{1}{2}}$-$7^2P_{\frac{1}{2}}$ FORBIDDEN M1TRANSITION IN THALLIUM

David B. Neuffer

Physics Department, University of California
Berkeley, California 94704
and
Materials and Molecular Research Division
Lawrence Berkeley Laboratory
Berkeley, California 94720

ABSTRACT

Calculations are presented of the E1 amplitude expected in forbidden M1 transitions of Tℓ and Cs if parity is violated in the neutral weak e-N interaction, as proposed in a number of gauge models, including that of Weinberg and Salam. Valence electron wave functions are generated as numerical solutions to the Dirac equation in a modified Tietz central potential. These wave functions are used to calculate allowed E1 transition rates, hfs splittings, and Stark E1 transition amplitudes. These results are compared with experiment and the agreement is generally good.

The relativistic Tℓ $6^2P_{\frac{1}{2}}$ - $7^2P_{\frac{1}{2}}$ M1 transition amplitude $\mathcal{M}$ is also calculated and corrections due to interconfiguration interaction, Breit interaction, and hfs mixing are included. The result:

$$\mathcal{M}_{theo} = (-3.2 \pm 1.0) \cdot 10^{-5} \frac{|e|\hbar}{2m_e c}$$

is in agreement with the experimental value:

$$\mathcal{M}_{expt} = (-2.11 \pm 0.30) \cdot 10^{-5} \frac{|e|\hbar}{2m_e c}$$

The parity violating E1 amplitude $\mathcal{E}_{PV}$ is calculated and a value for the circular dichroism in the Weinberg model

$$\delta = \frac{2\mathrm{Im}(\mathcal{E}_{PV})}{\mathcal{M}_{expt}} = -2.6 \times 10^{-3}$$

is obtained. Parity violating effects in other Tℓ transitions are discussed.

Contributions to the M1 amplitude for the forbidden Cs $6^2S_{1/2} - 7^2S_{1/2}$ and $6^2S_{1/2} - 8^2S_{1/2}$ transitions and to the Cs $6^2S_{1/2}$ g-factor anomaly from relativistic effects, Breit interaction, interconfiguration interaction, and hfs mixing are calculated, and it is found that this current theoretical description is not entirely adequate. The parity violating E1 amplitude $\mathcal{E}_{PV}$ for the $6S_{1/2}$-$7^2S_{1/2}$ and $6S_{1/2}$-$8^2S_{1/2}$ transitions is evaluated. The results

$$\mathcal{E}_{PV}(6^2S_{1/2} - 7^2S_{1/2}) = i\ 3.50 \cdot 10^{-11}\ Q_W\ |\mu_B|$$

$$\mathcal{E}_{PV}(6^2S_{1/2} - 8^2S_{1/2}) = i\ 1.48 \cdot 10^{-11}\ Q_W\ |\mu_B|$$

are obtained. With a measured value $\mathcal{M}_{expt}$ and the Weinberg value $Q_W = -99$, we find a circular dichroism $\delta = 1.64 \times 10^{-4}$ for the $6^2S_{1/2}$-$7^2S_{1/2}$ transition.

ACKNOWLEDGMENTS

I would like to thank Eugene D. Commins for his guidance, active participation and continuing support in this work. I would also like to thank Charles Schwartz and Peter Mohr for many important and helpful discussions. I also thank Steven Chu for useful discussions and for preparing Figure 1. I appreciate the continuing experimental efforts of Commins, Chu, Ralph Conti and Philip Bucksbaum.

I. CALCULATION OF PARITY VIOLATING EFFECTS IN THE $6^2P_{\frac{1}{2}} - 7^2P_{\frac{1}{2}}$ FORBIDDEN M1 TRANSITION IN THALLIUM

1. INTRODUCTION

Discovery of strangeness-conserving neutral weak currents in neutrino-nucleon scattering experiments[1] has stimulated considerable interest in the possible existence of a weak neutral electron-nucleon interaction. If such an interaction violates parity, as predicted by several theoretical gauge models including that of Weinberg and Salam (W-S), effects in heavy atoms such as optical rotation in allowed M1 transitions, and circular dichroism (dependence of absorption on photon helicity) in forbidden M1 transitions may be observable.

An experiment to study the latter effect in the doubly forbidden M1 transition $6^2P_{1/2}$-$7^2P_{1/2}$ (292.7 nm.) in atomic Tl vapor has been proposed.[3] The idea, originally suggested for the $6^2S_{1/2}$-$7^2S_{1/2}$ transition in Cs by Bouchiat and Bouchiat,[4] is that a short range, parity violating, neutral weak interaction H_{PV} mixes the $6^2P_{1/2}$,$7^2P_{1/2}$ Tl states with $n^2S_{1/2}$ states. Thus the transition $6^2P_{1/2}$-$7^2P_{1/2}$, nominally M1 with amplitude

$$\mathcal{M} = \langle 7^2P_{1/2}, m_J | M1 | 6^2P_{1/2}, m_J \rangle \qquad (1)$$

also contains a parity-violating electric dipole component with amplitude $\mathcal{E}_{PV} = \langle 7^2P_{1/2}, m_J | E1 | 6^2P_{1/2}, m_J \rangle$. It can be shown that interference between $\mathcal{M}$ and $\mathcal{E}_{PV}$ results in a dependence of the $6^2P_{1/2}$-$7^2P_{1/2}$ absorption rate W on right (R) or left (L) handed photon helicity:

$$\delta = \frac{W(R) - W(L)}{W(R) + W(L)} = \frac{2\,\mathrm{Im}(\mathcal{E}_{PV})\cdot\mathcal{M}}{|\mathcal{M}|^2 + |\mathcal{E}_{PV}|^2} \approx \frac{2\,\mathrm{Im}(\mathcal{E}_{PV})}{\mathcal{M}} \qquad (2)$$

The "circular dichroism" δ can be detected by observing the fluorescence accompanying decay of the $7^2P_{1/2}$ state (see Fig. 1). The first step in

that experiment was the determination of the M1 amplitude itself, the result being:[3]

$$\mathcal{M}_{expt} = (-2.11 \pm 0.30) \cdot 10^{-5}\ \mu_B \qquad (3)$$

where $\mu_B = |e|\hbar/2m_e c$. In that measurement and also in the experiment proposed to detect δ, use is made of the interference which occurs between $\mathcal{M}$ and/or $\mathcal{E}_{PV}$ and the Stark-induced electric dipole amplitude $\mathcal{E}_S$ for $6^2P_{\frac{1}{2}}$-$7^2P_{\frac{1}{2}}$ transitions in an external electric field.

In this paper we present results of calculations of the atomic structure of Tl which are necessary in order to make useful comparisons between these experiments and the predictions of models of the neutral weak interaction. The thallium atom has 81 electrons with a ground state electronic configuration: $1s^2 \ldots 5d^{10}\ 6s^2 6p$. Our approach is to assume that all singly-excited Tl I states of interest have the same inner electron configuration ($1s^2 \ldots 5d^{10} 6s^2$, with total L=0, S=0) as that of the ground state, and differ only in the valence electron orbital. This approximation, while not strictly correct, is reasonable, since inner shell ionization energies are at least several times larger than that of the 6p valence electron. It also has the obvious virtue of simplicity, since within such an approximation most properties of interest to us can be calculated from the valence electron wave-function, which is obtained by solving the Dirac equation numerically in a spherically symmetric potential, for all states of interest. We have chosen the potential:

$$V(r) = -\frac{e^2(Z-1)}{r(1+\eta r)^2}\, e^{-\gamma r} - \frac{e^2}{r} \qquad (4)$$

Without the exponential shielding factor $e^{-\gamma r}$, V(r) is the "Tietz" potential,[5] which yields a good approximate solution to the Thomas-Fermi equation. The factor $e^{-\gamma r}$ is inserted to account for the exponential decrease of electron density for large r. Parameters η and γ are chosen so that the calculated and observed $6^2P_{1/2}$ and $7^2P_{1/2}$ energies agree.

We describe calculations of energy levels, allowed E1 oscillator strengths, and $P_{1/2}$, $S_{1/2}$ hyperfine structure splittings, all in good agreement with observations (see Section 2). As is well known, the $6^2P_{3/2}$ hfs splitting is strongly affected by interconfiguration interaction, and a correction for this must be applied in order to obtain reasonable agreement with experiment (see Appendix A). Our calculation of $\mathcal{M}$ (Section 3) includes the one-electron relativistic contribution and corrections due to interconfiguration, hyperfine, and Breit interactions; the result is in agreement with the experimental value (Eq. 3). Our calculation of the Stark transition amplitudes $\mathcal{E}_S$ yields two second-order matrix elements α,β for linearly polarized excitation light parallel and perpendicular, respectively, to the applied static field E. The ratio β/α is in agreement with the experimental results of Chu, Commins, and Conti[3] (see Section 5).

The satisfactory agreement between experiment and the calculations described in the previous paragraph provide confidence that our estimate of the parity violating amplitude $\mathcal{E}_{PV}$ should be reliable enough

so that future experimental determinations of circular dichroism may yield useful tests of gauge models. For purposes of the present discussion we present the analysis in terms of the W-S model,[2] which describes low-energy strangeness conserving neutral weak interactions in terms of an effective Hamiltonian density:

$$\mathcal{H}(x) = \frac{G}{\sqrt{2}} J_\lambda(x) \cdot J^\lambda(x) \tag{5}$$

where G is the Fermi coupling constant of weak interactions; $G = 3 \times 10^{-12}$ in units ($\hbar = m_e = c = 1$) used throughout. The current $J^\lambda(x)$ has both hadronic and leptonic parts, the former being expressible as:

$$J^\lambda_{had} = V^{\lambda,0} + A^{\lambda,0} - 2 \sin^2\theta_w J^{\lambda,EM} \tag{6}$$

where $V^{\lambda,0}$ is the I_3 component of the strangeness-conserving hadronic vector current, $A^{\lambda,0}$ is the neutral $\Delta S=0$ hadronic axial current, $J^{\lambda,EM}$ is the EM current, and θ_w is the so-called "Weinberg" angle, which is given by $\sin^2\theta_w \cong 0.3$. That portion of the neutral leptonic current involving e^- is:

$$J^{lept,e^-}_\lambda = -\frac{1}{2}\left[(1 - 4\sin^2\theta_w)\,\bar{\Psi}_e \gamma_\lambda \Psi_e + \bar{\Psi}_e \gamma_\lambda \gamma_5 \Psi_e\right] \tag{7}$$

where Ψ_e is the electron field operator.

The first and second terms on RHS are respectively vector and axial-vector currents. We are interested in those portions of $\mathcal{H}(x)$ which are pseudoscalar, not scalar; thus we consider the product of the axial portion of J^{lept,e^-}_λ and the vector portion of J^λ_{had}. (The other pseudoscalar term corresponding to the product of the vector part of J^{lept,e^-}_λ and the axial part of J^λ_{had} gives a much smaller contribution since it is

proportional to total nuclear spin, and for a heavy nucleus, most of the nucleon spins cancel in pairs.) Ignoring this latter portion, we find:

$$\mathcal{H}^{PV}(x) \cong -\frac{G}{\sqrt{2}}\bar{\psi}_e\gamma_\lambda\gamma_5\psi_e \cdot (V^{\lambda,0} - 2\sin^2\theta_W J^{\lambda,EM}) \tag{8}$$

Taking matrix elements of $\mathcal{H}^{PV}(x)$ for the static limit of the nucleus, we obtain the matrix element of the effective Hamiltonian:

$$\langle H^{PV}\rangle = -\frac{GQ_W}{2\sqrt{2}}\,\psi_2^*(\vec{x})\,\gamma_5\psi_1(\vec{x})\Big|_{x=0} \tag{9}$$

where

$$Q_W = (1 - 4\sin^2\theta_W)\,Z - N \tag{10}$$

and $\psi_1(\vec{x})$, $\psi_2(\vec{x})$ are Dirac wave-functions corresponding to states of opposite parity, and "x=0" indicates the product is averaged over the nuclear volume. In fact, only $P_{\frac{1}{2}}$ and $S_{\frac{1}{2}}$ states yield non-negligible matrix elements. Equation (9) is derived from the W-S model. However, other gauge models with parity violation would lead to the same expression with only Q_W of Eq. (10) being model dependent. In most cases $|Q_W| \sim Z$. In Section 4 we use Eq. (9) to calculate $\mathcal{E}_{PV}$. Finally, Section 6 contains an estimate of parity violating effects for transitions in Tl other than $6^2P_{\frac{1}{2}}$-$7^2P_{\frac{1}{2}}$.

2. THALLIUM WAVE FUNCTIONS IN THE ONE ELECTRON CENTRAL FIELD APPROXIMATION

2.1 Construction of Wave Functions

The Dirac equation is

$$[\vec{\alpha}\cdot\vec{p} + \beta - eV]\psi = (1 - E_I)\psi \tag{11}$$

where E_I is the valence electron ionization energy [$(1 - E_I)$ is the total

electron energy including rest mass], and $\vec{\alpha}$ and β are the usual Dirac matrices. We write

$$\psi = \begin{pmatrix} \frac{f(r)}{r} \chi^{\mu}_{\kappa} \\ \frac{ig(r)}{r} \chi^{\mu}_{-\kappa} \end{pmatrix} \tag{12}$$

As usual, $\kappa = \mp(j+\frac{1}{2})$ for even(odd) parity states, the $\chi^{\mu}_{\pm\kappa}$ are two-component angular momentum-spin functions[6] given by:

$$\chi^{\mu}_{\kappa}(\theta,\phi) = \begin{pmatrix} C(\frac{1}{2},\ell,j;\ \frac{1}{2},\mu-\frac{1}{2},\mu)\ Y^{\mu-\frac{1}{2}}_{\ell}(\theta,\phi) \\ C(\frac{1}{2},\ell,j;-\frac{1}{2},\mu+\frac{1}{2},\mu)\ Y^{\mu+\frac{1}{2}}_{\ell}(\theta,\phi) \end{pmatrix} \tag{13}$$

the C's are Clebsch - Gordan coefficients, $\mu \equiv m_j$, $\ell = |\kappa + \frac{1}{2}| - 1$, and the Y's are spherical harmonics. Equation (12) reduces to the two coupled radial equations:

$$\begin{aligned} \frac{df}{dr} &= -\frac{\kappa}{r} f + [2 - E_I - V(r)]g \\ \frac{dg}{dr} &= \frac{\kappa}{r} g + [E_I + V(r)]f \end{aligned} \tag{14}$$

Following the procedure used by Schwartz[7] to calculate hyperfine structure splittings in Tl and other heavy atoms, we choose for V(r) the modified Tietz potential of Eq. (4). Parameters η and γ are chosen so that calculated and observed $6^2P_{\frac{1}{2}}$ and $7^2P_{\frac{1}{2}}$ energies agree. The fitting procedure is as follows:

(1) For very small r ($r \leq r_0 = 0.02 \frac{\hbar}{m_e c} = 0.02$), i.e. for r within the nuclear radius r_0, one of the following three potentials is chosen:

a) $V(r) = \frac{-Ze^2}{r}$ (Point nucleus)

b) $V(r) = \frac{-Ze^2}{r_0}$ (Constant potential)

c) $V(r) = \frac{Ze^2}{2r_0}\left(\frac{r^2}{r_0^2} - 3\right)$ (Constant nuclear charge density)

The initial wave-function values for this region are generated using a power series expansion to solve Eq. (14).

(2) For $r \geq r_0$ Eqs. (14) for f(r), g(r) are integrated numerically stepwise using a fourth order Runge-Kutta method.[8] Approximately 5000 intervals of length increasing from 0.001% to 2.0% are used.

(3) The eigenvalue condition is that $\lim_{r\to\infty} f(r) = 0$. The energy E_I in Eqs. (14) is varied to insure that this condition is satisfied.

The energy spectrum does not depend strongly on the choice of potential in step (1). Of all the quantities computed below, only the weak electron-nucleus interaction depends significantly on this choice, and for that quantity the dependence is only ~ 10%. The number of intervals can be reduced substantially without significant loss of precision except for calculation of the forbidden M1 transition (see Sec. 3); however this reduction would provide no economic advantage on the LBL CDC 7600 computer. The calculation procedure can be reversed by

choosing an asymptotic form for f and g at large r, and integrating step-wise toward r = 0. This yields the same states as the procedure actually used, but is less convenient for calculation of $\mathcal{E}_{PV}$.

The values of η and γ chosen for most calculations are

$$\eta = 2.5937 a_0^{-1} = 355.43\ \text{Å}^{-1}$$
$$\gamma = 0.2579 a_0^{-1} = 35.34\ \text{Å}^{-1} \qquad (15)$$

Numerical values of $\frac{f}{r}$ and $\frac{g}{r}$ versus r are given for several states of Table 1. These values are chosen to yield agreement between calculated and observed $6^2P_{\frac{1}{2}}$, $7^2P_{\frac{1}{2}}$ energy levels to within 0.1%. Other low lying $S_{\frac{1}{2}}$, $D_{\frac{1}{2}}$, $P_{\frac{1}{2}}$, and $P_{\frac{3}{2}}$ energy levels are calculated, and these all agree with observations to within 2%. Table II includes a comparison of calculated and observed energy levels.

2.2 Hyperfine Structure

The one-electron central-field (OECF) wave functions described above can be used to calculate hyperfine structure splittings for comparison with experimental values. This comparison provides a reasonably sensitive test of the accuracy of calculations of $\mathcal{E}_{PV}$ since both the latter and the hfs depend on values of the wave-functions near the origin. The perturbation Hamiltonian for hfs is

$$H_{hfs} = e\vec{\alpha}\cdot\vec{A} = e\vec{\alpha}\cdot\frac{\vec{m}_n\times\vec{r}}{r^3} = e\vec{m}_n\cdot\frac{\vec{r}\times\vec{\alpha}}{r^3} \qquad (16)$$

where $\vec{m}_n = g_n\mu_n\vec{I}$ is the nuclear magnetic moment operator, μ_n is the nuclear Bohr magneton, and $I = \frac{1}{2}$ is the spin for both stable thallium isotopes, ^{203}Tl and ^{205}Tl. Also $g_n(^{203}Tl) = 3.223$, $g_n(^{205}Tl) = 3.255$;[9]

in our calculations these are averaged to $g_n = 3.24$. It can then be shown that the hfs energy splittings are given in first-order by[6]:

$$\Delta W = e g_n \mu_n (J + \tfrac{1}{2}) \cdot \frac{8\kappa}{4\kappa^2 - 1} \cdot R \tag{17}$$

where

$$R = \int_0^\infty \frac{fg}{r^2}\, dr \tag{18}$$

Table II includes a list of hfs splittings calculated for the various energy levels, together with experimental values where these are available. The discrepancies are not due to major defects in the wave functions, but rather to interconfiguration interaction, which is known to have an especially large effect on the $6^2P_{3/2}$ state. This is demonstrated in Appendix A which contains an estimate of interconfiguration interaction for 6p electron states. Although the effect on the $6^2P_{3/2}$ hfs splitting is large it can be shown that interconfiguration interaction corrections to $\mathcal{E}_{PV}$ are negligible.

2.3 Fine Structure

Another test of the wave-function for small r is the fine structure splitting $\Delta E_{FS} = E(j = \ell + \tfrac{1}{2}) - E(j = \ell - \tfrac{1}{2})$ for $\ell \neq 0$. Non-relativistically,

$$\Delta E_{FS} = (\ell + \tfrac{1}{2}) \langle n\ell | \frac{1}{r} \frac{dV}{dr} | n\ell \rangle$$

In a relativistic calculation such as ours, the fine structure is part of the unperturbed Hamiltonian, and the calculated fine structure is simply the difference between calculated $(j = \ell + \tfrac{1}{2})$ and $(j = \ell - \tfrac{1}{2})$ energy levels. Comparison of these differences with observed energy differences from Table II for P states yields discrepancies $\lesssim 15\%$.

An alternative strategy of choosing V(r) by requiring ΔE_{FS} to agree for 6P states introduces 10% errors in the excited state energies and unacceptable (~2×) errors in electric dipole matrix elements.

2.4 Allowed Electric Dipole Transitions

We also calculate electric dipole radial integrals and transition strengths using the OEDF wave-functions. In the relativistic notation of Berestetskii, Lifschitz, and Pitaevskii,[10] the transition matrix element is

$$V_{fi} = e \int d^3\vec{r}\; j^{\mu}_{fi}\,(\vec{r})\; A^{*}_{\mu}\,(\vec{r}) \tag{19}$$

where $j^{\mu}_{fi}\,(r) = \bar{\psi}_f\, \gamma^{\mu}\, \psi_i$ is written in terms of the initial and final Dirac wave-functions ψ_i, ψ_f, γ^{μ} are the standard 4×4 matrices, and $A_{\mu}\,(\vec{r})$ is the 4-vector potential. In the long-wavelength approximation for an electric multipole field of order J,M we have:

$$A_{\mu}\,(\vec{r}) = \left(A_o\,(\vec{r}),\ 0,\ 0,\ 0\right)$$

$$A_o\,(\vec{r}) = -\int \frac{d^3\vec{k}}{(2\pi)^3} \sqrt{\frac{J+1}{J}}\; \frac{4\pi^2}{\omega^{3/2}}\; \delta(|\vec{k}| - \omega)\; Y^M_J\left(\frac{\vec{k}}{\omega}\right) \cdot e^{i\vec{k}\cdot\vec{r}}$$

$$\cong r^J\,(-1)^{M+1}\, i^J \sqrt{\frac{J+1}{J}}\; \frac{2\omega^{J+\frac{1}{2}}}{(2J+1)!!}\; Y^M_J\left(\frac{\vec{r}}{r}\right) \tag{20}$$

For E1 radiation, this becomes:

$$A_o\,(\vec{r}) = (-1)^{M+1} \cdot i \cdot r \cdot \frac{2\sqrt{2}}{3}\; \omega^{3/2}\; Y^M_1\left(\frac{\vec{r}}{r}\right) \tag{21}$$

Combining Eqs. (19) and (21) we obtain:

$$V_{fi}^{1,M} = (-1)\ i\ \omega^{3/2}\ \frac{2\sqrt{2}}{3}\int d^3\vec{r}\ \ \psi_f^*(\vec{r})\ r\ Y_1^{M*}\left(\frac{\vec{r}}{r}\right)\ \psi_i(\vec{r}) \qquad (22)$$

The spontaneous emission rate A is given by:

$$A_{fi} = 2\pi\ \overline{V_{fi}^2}$$

where $\overline{V_{fi}^2}$ is V_{fi}^2 summed over photon states and final electron states (j_f, m_f), and averaged over initial electron states (j_i, m_i). For OBCF wave-functions the angular integration is easily separated and we find the following:

Transition	A-coefficient
$S_{1/2} \rightarrow P_{1/2}$, $D_{3/2} \rightarrow P_{1/2}$	$4/9\ e^2\ \omega^3\ \langle r\rangle_{fi}^2$
$S_{1/2} \rightarrow P_{3/2}$	$8/9\ e^2\ \omega^3\ \langle r\rangle_{fi}^2$
$D_{3/2} \rightarrow P_{3/2}$	$4/45\ e^2\ \omega^3\ \langle r\rangle_{fi}^2$
$D_{5/2} \rightarrow P_{3/2}$	$8/15\ e^2\ \omega^3\ \langle r\rangle_{fi}^2$

where ω is the observed energy difference between initial and final states, and $\langle r\rangle_{fi} = \int r(f_f f_i + g_f g_i)dr$. The signs of these radial integrals are fixed by the convention that $f(r) > 0$ as $r \rightarrow 0$ for every state. In Table III, the radial integrals $\langle r\rangle_{fi}$ and calculated A-coefficients for nD → 6P and nS → 6P transitions are listed, together with observed A coefficients for the same transitions as determined by Gallagher and Lurio.[11] The agreement between theory and experiment is generally good, the discrepancy in the transition rates typically being ≲ 20%. This corresponds to a discrepancy in the

radial integrals of $\lesssim 10\%$, and reveals that our wave functions are reasonably accurate in the range $r \geq 2\text{Å}$.

The oscillator strengths F_{fi} are defined by

$$F_{fi} = \left(\frac{2J_f + 1}{2J_i + 1} \right) \frac{A_{if}}{2c^2 \omega^2} \tag{23}$$

where J_i, J_f are the initial and final total electronic angular momenta. These quantities have previously been calculated by Anderson et al.[12] by a method similar to ours (one-electron Dirac wave-function and central potential). Table III includes a comparison of their calculated oscillator strengths with ours for $nD \rightarrow 6P$ and $nS \rightarrow 6P$ transitions. Table IV gives the same comparison for $7P \rightarrow nS$ and $7P \rightarrow nD$ transitions, the radial integrals for which are needed in evaluation of $\mathcal{E}_{PV}$ and $\mathcal{E}_S$ (see Sections 4 and 5). Our calculated oscillator strengths and those of Anderson et al. are nearly identical, which suggests that the discrepancies ($\lesssim 20\%$) between calculated and observed values are due to a failure of the OECF approximation, rather than merely to an inadequate central potential. Thus to obtain more accurate results it may be necessary to go beyond the simple OECF model.

3. MAGNETIC DIPOLE TRANSITION RATES

3.1 The Relativistic Contribution

The relativistic contribution to $\mathcal{M}$ arises from the transition matrix element:[10]

$$V_{fi} = i\, e \sqrt{2\omega} \int d^3 r \quad \psi_f^*(\vec{r})\, \vec{\alpha}\, \psi_i(\vec{r}) \cdot \left[\frac{\vec{r} \times \vec{\nabla}}{\sqrt{2}} Y_{1m}^* \right] g_1(kr) \tag{24}$$

where $g_l(kr) = \sqrt{\frac{\pi}{2kr}}\, J_{3/2}(kr)$ is a spherical Bessel function. Using Eq. (12) for ψ_i, ψ_f which are both $P_{1/2}$ states, employing $\vec{\alpha} = \begin{pmatrix} 0 & \vec{\sigma} \\ \vec{\sigma} & 0 \end{pmatrix}$ and $(\vec{\sigma}\cdot\vec{r}/r)\chi_1^\mu = -\chi_{-1}^\mu$, and utilizing the anti-commutation of $\vec{\sigma}\cdot\vec{r}/r$ and $\vec{\sigma}\cdot\vec{\nabla}\,Y_{lm}$, we obtain

$$V_{fi} = -\,i\,e\sqrt{2\omega}\int dr\; g_1(kr)\,(f_f g_i + f_i g_f)\cdot \int r\,d\Omega\;\chi_{-1}^{\mu_f}\;\vec{\sigma}\cdot\vec{\nabla}\,Y_{lm}^{*}\;\chi_{-1}^{\mu_i} \tag{25}$$

We rewrite this as

$$V_{fi} = (-1)^m\sqrt{2/3\pi}\;\;\omega^{3/2}\;\;\vec{\mu}_{fi}\cdot\hat{\epsilon}_m \tag{26}$$

where $\hat{\epsilon}_m$ is the spherical unit vector:

$$\hat{\epsilon}_m = \vec{\nabla}\,(\sqrt{4\pi/3}\;r\;Y_{lm}) \tag{27}$$

and

$$\vec{\mu}_{fi}\cdot\hat{\epsilon}_m = -e\int dr\; g_1\frac{(kr)}{\omega}\,(f_f g_i + g_f f_i)\cdot \int d\Omega\;\;\chi_{-1}^{\mu_f *}\;\vec{\sigma}\cdot\vec{\nabla}\;\sqrt{4\pi/3}\;r\,Y_{lm}\,\chi_{-1}^{\mu_i} \tag{28}$$

for $P_{1/2} \to P_{1/2}$ transitions. The expression for $\vec{\mu}_{fi}\cdot\hat{\epsilon}_m$ in the case of $S_{1/2} - S_{1/2}$ transitions is the same except for a change in sign.

To find the transition rate

$$A = 2\pi\;\overline{|V_{fi}|^2} = \frac{4}{3}\omega^3\;\overline{|\vec{\mu}_{fi}\cdot\hat{\epsilon}_m|^2} \tag{29}$$

we sum over final and average over initial states to obtain:

$$A = 4\omega^3 e^2\left|\int\frac{g_1(kr)}{\omega}\;(f_f g_i + g_f f_i)dr\right|^2 \tag{30}$$

This formula was previously obtained by Johnson[13] for the $2^2S_{\frac{1}{2}} - 1^2S_{\frac{1}{2}}$ M1 transition in hydrogen. The result is also valid for allowed $\frac{1}{2} - \frac{1}{2}$ transitions. In this case $\vec{\mu}_{fi}$ of Eq. (28) approaches the familiar

$$\vec{\mu}_{fi} = \int \psi_f \left[\frac{e}{2} \vec{L} + \mu_e \frac{\vec{S}}{S} \right] \psi_i \, d^3r \tag{31}$$

in the non-relativistic limit. This expression vanishes if the radial parts of ψ_i and ψ_f are orthogonal.

We use our OECF radial wave-functions for $6^2P_{\frac{1}{2}}$, $7^2P_{\frac{1}{2}}$ states to compute the result:

$$\mathcal{M}_{REL} = -e \int \frac{g_1(kr)}{\omega} (f_i g_f + g_i f_f) dr = -1.757 \times 10^{-5} \ \mu_B \tag{32}$$

The extremely small size of this matrix element implies that relatively large corrections might occur due to interconfiguration mixing, hyperfine mixing, and the Breit interaction.

3.2 Interconfiguration Interaction Correction

Electrostatic interaction of the outer electron with excited core states alone (as in Appendix A) does not directly effect the M1 transition rate, since it mixes only those states having the same total L and S ($^2P_{\frac{1}{2}}$ in Tℓ).[14] However, in second order, Spin-orbit coupling allows an admixture of different L, S atomic s[illegible] (e.g. $^4P_{\frac{1}{2}}$ in Tℓ) and this admixture can give rise to a finite [illegible]mplitude even in the non-relativistic limit.

A consistent fourth order treatment is necessary; the calculation which follows is similar to that done by Phillips for corrections to $g_J(Cs)$.[14] Since the ground configuration of Tℓ is $(1s^2 \ldots .5d^{10}6s^26p)$,

we only consider the effects of 6s-electron excitation (the correction due to 5d excitation turns out to be smaller). The unperturbed states are

$$\psi_6 \equiv \psi(6^2P_{1/2}) = 6s^2(^1S_0)\ 6p\ ^2P_{1/2}$$
$$\psi_7 \equiv \psi(7^2P_{1/2}) = 6s^2(^1S_0)\ 7p\ ^2P_{1/2} \tag{33}$$

The first-order perturbation is the electrostatic interaction and the perturbing states considered are:

$$\Phi_6 = 6s7s(^3S_1)\ 6p\ ^2P_{1/2}$$
$$\Phi_7 = 6s7s(^3S_1)\ 7p\ ^2P_{1/2} \tag{34}$$

Thus the perturbed states are

$$\psi_6 = \psi_6 + \alpha_6\Phi_6 + \alpha_7\Phi_7$$
$$\psi_7 = \psi_7 + \beta_6\Phi_6 + \beta_7\Phi_7 \tag{35}$$

where α_6, α_7, β_6, β_7 are calculated by first order perturbation theory, and antisymmetrization of the total wave function is taken into account. For example:

$$\alpha_6 = -\sqrt{3/2}\ G_1 \frac{(6s,\ 6p;\ 7s,\ 6p)}{\Delta E}$$

where $G_1(6s,\ 6p;\ 7s,\ 6p)$ is the exchange electrostatic integral, $\Delta E = E(\Phi_6) - E(\psi_6)$, and $E(\Phi_6)$ is a fictitious energy calculated for a 6s7s6p configuration in the potential of Eq. (4). Numerical computation gives:

$$\alpha_6 = -0.010,\quad \alpha_7 = +0.023,\quad \beta_6 = 0.094,\quad \beta_7 = 0.006\ . \tag{36}$$

The $6s7s(^3S_1)np\ ^2P_{1_2}$ states are now mixed with states

$$\phi_n'(^4P_{1_2}) = 6s7s(^3S_1)\ n'p\ ^4P_{1_2} \tag{37}$$

by spin-orbit interaction. We employ the perturbation Hamiltonian

$$H' = \sum_i \xi_i \vec{L}_i \cdot \vec{S}_i = \frac{1}{2} \sum_i \left(\frac{1}{r}\ \frac{\partial V}{\partial r}\right)_i \vec{L}_i \cdot \vec{S}_i \tag{38}$$

and rewrite our wave functions as

$$\begin{aligned}\psi_6' = \psi_6 &+ \alpha_6[\phi_6 + a_6\phi_6'(^4P_{1_2}) + a_7\phi_7'(^4P_{1_2})] \\ &+ \beta_6[\phi_7 + b_6\phi_6'(^4P_{1_2}) + b_7\phi_7'(^4P_{1_2})]\end{aligned} \tag{39}$$

and

$$\begin{aligned}\psi_7' = \psi_7 &+ \alpha_7[\phi_6 + c_6\phi_6'(^4P_{1_2}) + c_7\phi_7'(^4P_{1_2})] \\ &+ \beta_7[\phi_7 + d_6\phi_6'(^4P_{1_2}) + d_7\phi_7''(^4P_{1_2})]\end{aligned} \tag{40}$$

The coefficients $a_6,\ldots d_7$ are calculated from the observed P-state fine structure splitting. For example,

$$a_6 = -\frac{2\sqrt{2}}{9} \cdot \frac{[E(6^2P_{3/2}) - E(6^2P_{1_2})]}{\Delta E} \tag{41}$$

where $\Delta E = E(\psi_6) - E(\phi_6')$. We find: $a_6 = +0.033$, $a_7 = +0.0081$, $b_6 = +0.012$, $b_7 = +0.0029$, $c_6 = +0.061$, $c_7 = +0.012$, $d_6 = +0.022$, $d_7 = 0.0043$. The interconfiguration interaction correction to $\mathcal{M}$ is now computed from Eqs. (39), (40) by means of the formula

$$\mathcal{M}_{II} = \langle\psi_6'|M1|\psi_7'\rangle - \mathcal{M}_{REL} \tag{42}$$

In the evaluation of all the perturbing terms we use the non-relativistic form (31). We find:

$$\mathcal{M}_{II} = [(\alpha_7 c_6 + \beta_7 d_6)(\alpha_6 a_6 + \beta_6 b_6) + (\alpha_7 c_7 + \beta_7 d_7)(\alpha_6 a_7 + \beta_6 b_7)] \cdot \tfrac{1}{4}[g(^4P_{\frac{1}{2}}) - g(^2P_{\frac{1}{2}})] \cdot \frac{e}{2} = -1.9 \times 10^{-6}\ \mu_B \tag{43}$$

Inclusion of higher s-state excitations (6s ns np) does not significantly change Eq. (43). However, since the electrostatic exchange integrals are fairly sensitive to small changes in wave-functions, the 4th order result (43) might be in error by as much as a factor of 2.

3.3 Breit Interaction Corrections

The OECF approximation used up to now does not include a complete description of electron-electron interactions, even if we assume a spherically symmetric core. To order v^2/c^2, the electron-electron interaction contributes a term to the Hamiltonian:

$$\Delta H = \sum_{i<k} \frac{e^2}{r_{ik}} - \frac{e^2}{2} \sum_{i<k} \left(\frac{\vec{\alpha}_i \cdot \vec{\alpha}_k}{r_{ik}} + \frac{(\vec{\alpha}_i \cdot \vec{r}_{ik})(\vec{\alpha}_k \cdot \vec{r}_{ik})}{r_{ik}^3} \right) \tag{44}$$

The first term on RHS of (44) is in fact partially included in the central potential (Eq. 4) but the second term is not, and must be regarded as an additional perturbation. This term may be reduced to the following expression (Breit interaction)[15]:

$$\Delta H_B = \frac{e^2}{2} \sum_{i \neq k} \left[\vec{\nabla}_i \frac{1}{r_{ik}} \times \vec{p}_i \right] \cdot \vec{\sigma}_k - \frac{e^2}{2} \sum_{i<k} \left[\frac{1}{r_{ik}} \vec{p}_i \cdot \vec{p}_k + \frac{1}{r_{ik}^3} (\vec{r}_{ik} \cdot (\vec{r}_{ik} \cdot \vec{p}_i) \cdot \vec{p}_k) \right] \tag{45}$$

In order to calculate the contribution of this interaction to the M1 transition we replace $\vec{p}$ by $\vec{p} + e\vec{A}$ (electron charge = -e), where $\vec{A} = \vec{B} \times \vec{r}/2$.

Thus we obtain:

$$\mathcal{M}_{B,\,eff} = \frac{e^3}{2} \sum_{i \neq k} \left(\vec{\nabla}_i \frac{1}{r_{ik}} \times \vec{A}_i \right) \cdot \vec{\sigma}_k \cdot \frac{e^3}{2} \sum_{i \neq k} \left[\frac{\vec{A}_i \cdot \vec{p}_k}{r_{ik}} + \frac{\vec{r}_{ik} \cdot \vec{A}_i \; \vec{r}_{ik} \cdot \vec{p}_k}{r_{ik}^3} \right] \tag{46}$$

This expression has been derived previously by Abragam and Van Vleck,[16] and Schwartz.[17] We now consider the special case of one electron outside a spherically symmetric electron distribution; it has been shown that only electrons outside of closed shells give non-vanishing contributions.[16]

It can then be shown that the matrix element of the first term on RHS of (46), called the "Lamb" correction,[18]

$$\mathcal{M}_L = -\frac{e^3}{2} \int \psi_1'^{*}(\vec{r}_1) \vec{\sigma}_1 \cdot \vec{\nabla}_1 \times \left[\int \frac{\vec{A}(r_2)\, \rho(\vec{r}_2) d\tau_2}{|\vec{r}_1 - \vec{r}_2|} \right] \psi_1 (\vec{r}_1)\, d\tau_1 \tag{47}$$

where $\rho(\vec{r}_2) = \sum_{k \neq 1} \psi_k^{*}(\vec{r}_2) \psi_k(\vec{r}_2)$

For present purposes we choose ψ_1, ψ_1' to be $6P_{\frac{1}{2}}$, $7P_{\frac{1}{2}}$ wave functions, respectively; for $\rho(\vec{r}_2)$ we insert the spherically symmetric density obtained from our central potential, and we set $\vec{B} \parallel z$. Then the amplitude for the $m_J = \frac{1}{2} \rightarrow m_{J'} = \frac{1}{2}$ transition is reduced to a sum of radial integrals:

$$\mathcal{M}_L = \frac{e}{2} B \left[-\frac{4e^2}{45} \langle V \rangle + \frac{e^2}{9} \langle W \rangle \right] \tag{48}$$

where

$$\langle V \rangle = \int_0^\infty \frac{F(r_1)}{r_1^3} \left[\int_0^{r_1} r_2^4 \, \rho(r_2) dr_2 \right] F'(r_1) \, r_1^7 \, dr_1 \tag{49}$$

and

$$\langle W \rangle = \int_0^\infty F(r_1) \left[\int_{r_1}^\infty \rho(r_2) r_2 \, dr_2 \right] F'(r_1) r_1^2 dr_1 \tag{50}$$

and F, F' are the non-relativistic 6p, 7p radial wave-functions, respectively. The resulting contribution to $\mathcal{M}$ is evaluated numerically to be (The $\langle V \rangle$ and $\langle W \rangle$ terms enter with opposite signs and largely cancel.)

$$\mathcal{M}_L = -4 \times 10^{-7} \, \mu_B \tag{51}$$

The second term on RHS of (46), called the "orbit-orbit" correction,[16] gives the following matrix element:

$$\mathcal{M}_{OR} = \frac{-e^3}{6} \int \psi_1^* (\vec{r}_1) \left[\frac{1}{r_1^3} \int_0^{r_1} \rho(r_2) \, r_2^4 dr_2 + \int_{r_1}^\infty \rho(r_2) r_2 \, dr_2 \, \vec{L}_1 \right] \times \vec{B} \psi_1' (\vec{r}_1) \, d^3 r_1 \tag{52}$$

For $\vec{B} \parallel \hat{z}$, $m_J = \frac{1}{2} \rightarrow m_J' = \frac{1}{2}$, this becomes:

$$\mathcal{M}_{OR} = \frac{-e^3 B}{9} \left[\langle W \rangle + \langle V \rangle \right] \tag{53}$$

which yields the following numerical contribution to $\mathcal{M}$

$$\mathcal{M}_{OR} = -1.20 \times 10^{-5} \, \mu_B \tag{54}$$

3.4 Total Theoretical M1 Rate; Corrections to $g_J(Tl, 6^2P_{1/2})$

We collect the four contributions to the M1 amplitude (Eqs. (32), (43), (51), and (54)):

$$\mathcal{M} = \mathcal{M}_{REL} + \mathcal{M}_{II} + \mathcal{M}_{L} + \mathcal{M}_{OR} = -3.2 \times 10^{-5} \ \mu_B \qquad (55)$$

Our analysis of hyperfine structure indicates that there is an uncertainty of ~20% in the calculation of relativistic effects. In addition, $\mathcal{M}_{II}$ has an independent uncertainty of $\sim 0.15\mathcal{M}$. The combined theoretical uncertainty of $\mathcal{M}$ (Eq. 55) is estimated to be $\sim 1.0 \times 10^{-5}\ \mu_B$.

The Zeeman energy shift in a constant magnetic field B_z is related to g_J by:

$$\Delta E = \mu_B g_J m_J B_z \qquad (56)$$

In zeroth order

$$g_J = \frac{J(J+1) + L(L+1) - S(S+1)}{2J(J+1)} + g_S \frac{J(J+1) + S(S+1) - L(L+1)}{2J(J+1)}$$

where $g_S = 2.002319114$. The corrections to g_J are obtained in the same manner as those described in Sections 3.1 - 3.3, merely by computing $6^2P_{1/2}$-$6^2P_{1/2}$ diagonal matrix elements. The results of this calculation are displayed in Table 5 and compared with experiment.[19] The agreement is very good. We expect an error of $\lesssim 15\%$ for δg from the same considerations mentioned above, modified slightly for $6^2P_{1/2} - 6^2P_{1/2}$ diagonal elements. The very close agreement (~3%) is, we believe, fortuitous.

3.5 Hyperfine Mixing

Next, we calculate the additional contributions to the M1 amplitude arising from admixture to 6P, 7P wave-functions of 7P, 6P components, respectively, due to hyperfine interaction. According to first order perturbation theory,

$$\overline{|6^2P_{\frac{1}{2}},F\rangle} = |6^2P_{\frac{1}{2}},F\rangle + \frac{\langle 7^2P_{\frac{1}{2}},F\,|H_{HFS}|\,6^2P_{\frac{1}{2}},F\rangle}{E_{6p} - E_{7p}}\,|7^2P_{\frac{1}{2}},F\rangle \tag{57}$$

$$\overline{|7^2P_{\frac{1}{2}},F'\rangle} = |7^2P_{\frac{1}{2}},F'\rangle + \frac{\langle 6^2P_{\frac{1}{2}},F'|\,H_{HFS}|\,7^2P_{\frac{1}{2}},F'\rangle}{E_{7p} - E_{6p}}\,|6^2P_{\frac{1}{2}},F'\rangle \tag{58}$$

where the $\overline{|\ldots\rangle}$ indicates a perturbed state, and H_{HFS}, given by Eq. (16), is diagonal in F, the total atomic angular momentum. This contributes to the M1 transition matrix element as follows:

$$\langle \overline{7^2P_{\frac{1}{2}},F'}\,|M1|\,\overline{6^2P_{\frac{1}{2}},F}\rangle_{HFS} \cong (\langle 7P,F\,|H_{HFS}|\,6P,F\rangle - \langle 6P,F'\,|H_{HFS}|7P,F'\rangle) \cdot \frac{1}{E_{6p}-E_{7p}} \cdot \langle nP_{\frac{1}{2}},F'\,|M1|\,nP_{\frac{1}{2}},F\rangle \tag{59}$$

where on the RHS we use the non-relativistic M1 operator, whose matrix elements are independent of principal quantum number n. It is interesting to note that the LHS of Eq. (59) vanishes for F = F'; thus this correction, unlike the previous ones, only affects F = 0 → F' = 1 and F = 1 → F' = 0 transitions. The hyperfine matrix elements on the RHS may be computed by the methods of Section 2.3 with the following results:

For $F = 0$, $F' = 1$,

$$M1^{F'=1,F=0}_{HFS} = +2.6 \times 10^{-6}\ \mu_B$$

For $F = 1$, $F' = 0$,

$$M1^{F'=0,F=1}_{HFS} = -2.6 \times 10^{-6}\ \mu_B \cdot \sqrt{\frac{1}{3}}$$

3.6 Other M1 Transitions

The methods outlined in Sections 3.1 - 3.3, and 3.5 may be used to calculate other T& M1 transitions, forbidden or allowed. These include the $6^2P_{\frac{1}{2}} - 6^2P_{\frac{3}{2}}$ transition (allowed) which has been suggested as an interesting candidate for a neutral current experiment, and the $6^2P_{\frac{1}{2}} - 7^2P_{\frac{3}{2}}$, $6^2P_{\frac{3}{2}} - 7^2P_{\frac{1}{2}}$ transitions which are not so strongly forbidden as $nP_{\frac{1}{2}} - n'P_{\frac{1}{2}}$ and $nP_{\frac{3}{2}} - n'P_{\frac{3}{2}}$ cases, since for $\frac{1}{2} \to \frac{3}{2}$ or $\frac{3}{2} \to \frac{1}{2}$, the radial wave functions are not fully orthogonal. In what follows we ignore the small higher-order effects considered in Sections 3,2, 3.3, and 3.5, and consider only the one-electron amplitude of Eq. (28). For $nP_{\frac{3}{2}} - nP_{\frac{1}{2}}$ transitions we find

$$A_{\frac{3}{2}\to\frac{1}{2}} = 2\pi\ |\overline{V_{fi}}|^2 = e^2\omega^3 \left| \int \frac{g_1(kr)}{\omega} \left(f_{\frac{3}{2}}g_{\frac{1}{2}} + g_{\frac{3}{2}}f_{\frac{1}{2}}\right) \right|^2$$

and similarly for $\frac{1}{2} \to \frac{3}{2}$ transitions. The results are tabulated in Table 6. In the allowed cases, the M1 matrix elements are within 2% of the non-relativistic value $-\sqrt{2}/3$, while the forbidden ($6^2P_{\frac{1}{2}} - 7^2P_{\frac{3}{2}}$, $6^2P_{\frac{3}{2}} - 7^2P_{\frac{1}{2}}$) matrix elements are about 10% of the allowed values, which corresponds to the expected magnitude of spin-orbit coupling effects.

These transitions also have non-zero electric quadrupole (E2) amplitudes. We obtain:

$$A_{E2} \cong \frac{1}{75}\, e^2\omega^5 \left[\int_0^\infty f_f\, r^2\, f_i\, dr\right]^2 \tag{63}$$

The portion of the E2 amplitude which is proportional to $\int g_f\, r^2 g_i\, dr$ is quite negligible. Table 6 includes a tabulation of the E2 radial integrals and resulting A coefficients. The coefficient A_{E2} $(6^2P_{3/2} \rightarrow 6^2P_{1/2})$ has also been calculated by Garstang[20] and his result (0.11 sec^{-1}) and ours are in agreement.

4. PARITY VIOLATING E1 AMPLITUDES

4.1 $6^2P_{1/2} \rightarrow 7^2P_{1/2}$ Transition

As previously discussed (Sec. 1) parity-violation in the electron-nucleon weak neutral interaction manifests itself in the matrix element:

$$\langle\psi_1|H_{PV}|\psi_2\rangle = \frac{-GQ_W}{2\sqrt{2}}\, \psi_1^*(\vec{x})\, \gamma_5 \psi_2(\vec{x})\Big|_{\vec{x}=0} \tag{64}$$

We write the perturbed 6P, 7P states as:

$$|\overline{6P_{1/2}}\rangle = |6P_{1/2}\rangle + \sum_n \frac{\langle nS_{1/2}|H_{PV}|6P_{1/2}\rangle}{E_{6P} - E_{nS}}\, |nS_{1/2}\rangle \tag{65}$$

$$|\overline{7P_{1/2}}\rangle = |7P_{1/2}\rangle + \sum_n \frac{\langle nS_{1/2}|H_{PV}|7P_{1/2}\rangle}{E_{7P} - E_{nS}}\, |nS_{1/2}\rangle \tag{66}$$

From (64) we obtain:

$$\langle nS_{1/2}|H_{PV}|n'P_{1/2}\rangle = \frac{i}{4\pi}\, \frac{G}{2}\, \frac{Q_W}{\sqrt{2}}\, \frac{1}{r^2} \left[f_{ns}(r)\, g_{n'p}(r) - f_{n'p}(r)\, g_{ns}(r)\right] \cdot \delta_{m_s m_p} \tag{67}$$

This expression is averaged over the nucleus assuming a constant proton- and neutron- density. As an alternative, one may assume a point-like nucleus, and evaluate $\langle nS|H_{PV}|n'P\rangle$ at the nuclear radius; this increases the numerical value by 6%. The E1 matrix element is obtained by evaluating:

$$\langle \overline{7P}_{\frac{1}{2}} |E1| \overline{6P}_{\frac{1}{2}} \rangle = \sum_{nS} \frac{\langle 7P_{\frac{1}{2}}|E1|nS\rangle \langle nS|H_{PV}|6P_{\frac{1}{2}}\rangle}{E_{6P} - E_{nS}} + \sum_{nS} \frac{\langle 7P_{\frac{1}{2}}|H_{PV}|nS\rangle \langle nS|E1|6P_{\frac{1}{2}}\rangle}{E_{7P} - E_{nS}} \tag{68}$$

For the E1 matrix elements on RHS of Eq. (68) we have

$$\langle nS|E1|P_{\frac{1}{2}}\rangle = e\langle nS|\hat{\varepsilon}\cdot r|P_{\frac{1}{2}}\rangle = e\int f_S r f_P \, dr \cdot \chi_{-1}^{m_S} \hat{\varepsilon}\cdot\hat{e}_r \chi_1^{m_P}$$
$$= \frac{e}{3}\int f_S f_P \, dr , \qquad (m_S = m_P = -\tfrac{1}{2}) \tag{69}$$

Expression (68) is evaluated by two methods:

1. A sum is taken over the lowest five states $|6s^2 ns\rangle$, $n > 6$; and the effect of the autoionizing $|6s\ 6p\ 7p\rangle$ state is also taken into account by including in the sum a term corresponding to the unphysical state $|6s^2\ 6s\rangle$. (See Appendix B for this argument.)

2. The operators $\sum_n \frac{|nS\rangle\langle nS|}{E_{n'p} - E_{nS}}$ are replaced by Dirac Green's functions, described in detail in Appendix C. This calculation includes the contribution of all intermediate S-states including continuum and autoionizing states and is thus more reliable and complete than method 1.

The results are summarized in Table 7. The Green's function method yields the numerical value for $\mathcal{E}_{PV} = \langle \overline{7P}_{\frac{1}{2}} | E1 | \overline{6P}_{\frac{1}{2}} \rangle$ in Eq. (68):

$$\mathcal{E}_{PV} = 1.93\, i \cdot 10^{-10}\, Q_w\, |\mu_B| \tag{70}$$

which corresponds to an A coefficient:

$$A = 1.20 \cdot 10^{-16}\, Q_w^2\ \text{sec}^{-1} \tag{71}$$

In the Weinberg model,

$$Q_w = Z\,(1 - 4\sin^2\theta_w) - N \cong -140 \tag{72}$$

for Tl, using $\sin^2\theta_w = 0.3$ as suggested by the experiment of Reines et al.[22] Thus we obtain from (70) and (72):

$$\mathcal{E}_{PV} = -2.70\, i \cdot 10^{-8}\, |\mu_B| \tag{73}$$

For the circular dichroism δ it can be shown that one obtains:

$$\delta = \frac{2\,\mathrm{Im}\,(\mathcal{E}_{PV})\mathcal{M}}{|\mathcal{M}|^2 + |\mathcal{E}|^2} \approx \frac{2\,\mathrm{Im}(\mathcal{E}_{PV})}{\mathcal{M}} \tag{74}$$

Inserting (73) and the experimental value of $\mathcal{M}$ from Eq. (3) into (74) we obtain:

$$\delta = -2.6 \cdot 10^{-3} \tag{75}$$

This result is to be compared with the calculation of Sushkov, Flambaum, and Khriplovich,[22] who obtain, also using $\mathcal{M}_{expt}$ from Eq. (3),

$$\delta = -2.5 \cdot 10^{-3} \tag{76}$$

To calculate $\mathcal{E}_{PV}$, they use non-relativistic hydrogenic wave-functions with an empirically determined correction factor. Their radial E1 integrals are extracted from experimental evidence where available, or from numerical calculations, and a finite sum over the five nearest levels is performed. It can be seen from Table VII that our complete Green's function evaluation differs from our finite sum by about 20%. The close agreement of Eqs. (75) and (76) is therefore somewhat fortuitous.

4.2 Other Parity-Violating Transitions

For $P_{1/2}$ - $P_{3/2}$ transitions we may ignore the effect of H_{PV} on the $P_{3/2}$ state since J = 3/2 wave functions have extremely small amplitudes at the nucleus. Thus,

$$\langle \widetilde{P_{3/2}} \,|E1|\, \widetilde{P_{1/2}} \rangle = \sum_{nS} \frac{\langle P_{3/2} \,|E1|\, nS\rangle\langle nS \,|H_{PV}|\, P_{1/2}\rangle}{E_{P_{1/2}} - E_{nS}} \tag{77}$$

These matrix elements were evaluated in the same way as described above for δ_{PV}. The results are summarized in Table 8, where

$$\langle P_{3/2} \,|E1|\, nS\rangle = \frac{e\sqrt{2}}{3} \int_0^\infty f_{P_{3/2}}\, r\, f_{S_{1/2}}\, dr \tag{77a}$$

5. STARK EFFECT

5.1 $6^2P_{1/2}$ - $7^2P_{1/2}$ Transitions

We now calculate the electric-field-induced E1 transitions which can occur between $6^2P_{1/2}$, $7^2P_{1/2}$ levels through Stark-mixing with $^2S_{1/2}$, $^2D_{3/2}$ states. The coordinate system is shown in Fig. 2. Action of the perturbation $H' = e\vec{E} \cdot \vec{r} = eE\, y$ results in the perturbed states:

$$\widetilde{|NP_{1/2}\rangle} = |NP_{1/2}\rangle + \sum_{nS} \frac{|nS\rangle\langle nS|\, eE_0 y\, |NP_{1/2}\rangle}{E_{NP_{1/2}} - E_{nS}}$$

$$+ \sum_{nD_{3/2}} \frac{|nD_{3/2}\rangle\langle nD_{3/2}\, |eE_0 y|\, NP_{1/2}\rangle}{E_{NP_{1/2}} - E_{nD_{3/2}}} \tag{78}$$

Thus an electric dipole transition stimulated by laser photons with linear polarization

$$\hat{\epsilon} = \cos\theta\, \hat{y} \quad \sin\theta\, \hat{z} \tag{79}$$

has amplitude:

$$\mathcal{E}_S = \langle \overline{7^2P_{1/2}} \,|E1|\, \overline{6^2P_{1/2}} \rangle_{Stark} =$$

$$n = S_{1/2},\ D_{3/2} \text{ states} \quad \left\{ \sum_n \frac{\langle 7^2P_{1/2}|e\hat{\epsilon}\cdot\vec{r}|n\rangle\langle n|eE_0 y|6^2P_{1/2}\rangle}{E_{6P_{1/2}} - E_n} + \sum_n \frac{\langle 7^2P_{1/2}|eE_0 y|n\rangle\langle n|e\hat{\epsilon}\cdot r|6^2P_{1/2}\rangle}{E_{7P_{1/2}} - E_n} \right. \tag{80}$$

The result of a calculation of this amplitude may be represented by a 2×2 matrix whose rows and columns are labelled by $m_J(6^2P_{1/2})$ and $m_J(7^2P_{1/2})$ respectively:

$$\mathcal{E}_S = e^2E_0 \cdot$$

$m_J(7^2P_{1/2})$	$m_J(6^2P_{1/2}) = \frac{1}{2}$	$m_J(6^2P_{1/2}) = -\frac{1}{2}$
$= \frac{1}{2}$	$\alpha\cos\Theta$	$-i\beta\sin\Theta$
$= -\frac{1}{2}$	$-i\beta\sin\Theta$	$\alpha\cos\Theta$

(81)

Here

$$\alpha = \frac{1}{9}\sum_{nS} R_{7P,nS}R_{6P,nS}\left(\frac{1}{E_7-E_{nS}} + \frac{1}{E_6-E_{nS}}\right) + \frac{2}{9}\sum_{nD_{3/2}} R_{7P,nD}\,R_{6p,nD}\left(\frac{1}{E_7-E_{nD}} + \frac{1}{E_6-E_{nD}}\right) \tag{82}$$

and

$$\beta = \frac{1}{9}\sum_{nS} R_{7P,nS}\,R_{6P,nS}\left(\frac{1}{E_6-E_{nS}} - \frac{1}{E_7-E_{nS}}\right) + \frac{1}{9}\sum_{nD_{3/2}} R_{7P,nD}\,R_{6P,nD}\left(\frac{1}{E_7-E_{nD}} - \frac{1}{E_6-E_{nD}}\right) \tag{83}$$

where $E_6 = E(6^2P_{\frac{1}{2}})$, $E_7 = E(7^2P_{\frac{1}{2}})$, and $R_{7P,nS} = \langle 7^2P_{\frac{1}{2}}|r|n^2S_{\frac{1}{2}}\rangle$, etc. The quantities α and β have been evaluated by summing over the nearest S and D states, and also by use of the Green's function, Appendix C. The results are summarized in Table 9.

Chu, Commins and Conti have measured β/α. Their result:[3]

$$\beta/\alpha]_{expt} = 0.84 \tag{84}$$

is in good agreement with the Green's function value of Table 9. These theoretical values of α and β were employed by them to determine the experimental value of $\mathcal{M}$ as described below.

5.2 Experimental Determination of M1 Amplitude

A finite $7^2P_{\frac{1}{2}}$ final state polarization can arise along the ? axis of Fig. 5.1 through interference between $\mathcal{M}$ and/or $\mathcal{E}_{PV}$ and $\mathcal{E}_S$. Interference between $\mathcal{M}$ and $\mathcal{E}_S$ may then be utilized to measure $\mathcal{M}$. Here the effects of $\mathcal{E}_{PV}$, which are in any case very small, are neglected. In an extension of this experiment now underway, interference between $\mathcal{E}_{PV}$ and $\mathcal{E}_S$ is utilized to determine $\mathcal{E}_{PV}$ itself.

In order to facilitate comparison with observations in which some of the hfs components of the $6^2P_{\frac{1}{2}} - 7^2P_{\frac{1}{2}}$ transition are resolved, we replace the matrix of Eq. (81) by one whose rows and columns are labelled by F', $m_{F'}$ (for $7^2P_{\frac{1}{2}}$) and F, m_F (for $6^2P_{\frac{1}{2}}$), respectively. Including $\mathcal{E}_{PV}$, $\mathcal{M}$ and $\mathcal{E}_S$, the total dipole amplitude D is given in Table 10.

In the experimental determination of $\mathcal{M}$, the $6^2P_{\frac{1}{2}}$ hfs splitting, but not that of $7^2P_{\frac{1}{2}}$, is resolved. Thus the $7^2P_{\frac{1}{2}}$ polarization is given by the formula:

$$P(F) = \frac{\sum_{m_F, m'_F} m_{F'} \left| D^{F', m_{F'}}_{F, m_F} \right|^2}{\sum_{m_F, m_F} \left| D^{F', m_{F'}}_{F, m_F} \right|^2} \qquad (85)$$

Neglecting $|\mathcal{H}|^2$ compared to $|\mathcal{E}_S|^2$ (which is justifiable for the rather large E fields employed) Eq. (84) becomes the following for the four indicated cases of interest:

a) $F = 1,\ F' = 1$ $\quad \hat{\epsilon} \parallel \vec{E}\ (\theta=0)$ $\quad P \cong \frac{4}{3}\frac{\mathcal{H}}{\alpha}$

b) $F = 0;\ F' = 0$ $\quad \hat{\epsilon} \parallel \vec{E}\ (\theta=0)$ $\quad P = 0$

c) $F = 1;\ F' = 1,0$ $\quad \hat{\epsilon} \perp \vec{E}\ (\theta=90°)$ $\quad P = -\frac{2}{3}\frac{\mathcal{H}}{\beta}$ ($7^2P_{\frac{1}{2}}$ hfs unresolved)

d) $F = 0;\ F' = 1$ $\quad \hat{\epsilon} \perp \vec{E}\ (\theta=90°)$ $\quad P = -2\frac{\mathcal{H}}{\beta}$

We now apply the hfs mixing correction of Eq. (60) to case d) (it also applies to case c but this was not observed in detail). The resulting ratio $P_d^{corr.}/P_a$ is then in good agreement with experiment. From their measurements of P_a and/or P_d Chu et al[3] obtain the experimental value of $\mathcal{H}$ given in Eq. (3).

5.3 Interference of $\mathcal{E}_{PV}$ and $\mathcal{E}_S$

When the incident light is circularly polarized, it becomes possible to measure the interference between $\mathcal{E}_{PV}$ and $\mathcal{E}_S$, again by detecting the polarization of the $7^2P_{\frac{1}{2}}$ state (by means of circular polarization of its decay fluorescence). The formulae analogous to Eq. (85) are readily obtained from Table 10. We quote only the result for the $F = 0 \rightarrow F' = 1$ transition:

$$P = \frac{\frac{1}{2}(\beta-f)^2 - \frac{1}{2}(\beta+f)^2}{\frac{1}{2}(\beta+f)^2 + \frac{1}{2}(\beta-f)^2 + f^2} \approx \frac{-2f}{\beta} \tag{86}$$

where $f = \mathcal{M} - \eta\mathcal{E}_{PV}$, $\eta = \pm 1$ for RHC (LHC) laser light, and the approximation $P \approx -2f/\beta$ is valid for large electric fields ($E \gg 1$ V/cm).

6. PARITY VIOLATION IN $^2P_{\frac{1}{2}} - {}^2P_{\frac{3}{2}}$ TRANSITIONS

For the transitions $6^2P_{\frac{1}{2}} - 6^2P_{\frac{3}{2}}$, $6^2P_{\frac{1}{2}} - 7^2P_{\frac{3}{2}}$, and $6^2P_{\frac{1}{2}} - 7^2P_{\frac{1}{2}}$, we include E2 as well as M1 contributions and write:

$$\langle T \rangle = \langle P_{\frac{3}{2}} | \vec{\mu} \cdot \overrightarrow{\hat{x} \times \hat{\epsilon}} + e\hat{\epsilon} \cdot \vec{r} + ie(\hat{\epsilon}\cdot\vec{r})(\vec{k}\cdot\vec{r}) | P_{\frac{1}{2}} \tag{87}$$

where $\vec{\mu} = e\hbar/2mc\ (\vec{L} + \vec{S})$, and $\hat{\epsilon} = \hat{y}\cos\Theta + \hat{z}\sin\Theta$.

The resulting transition matrix is given in Table 11. The polarization is calculated as in Eq. (86) with the result

$$P = \frac{2\mathcal{M} \cdot \mathrm{Im}(\mathcal{E}_{PV})}{|\mathcal{M}|^2 + \frac{2}{3}|\langle \mathcal{E}_2 \rangle|^2} \tag{88}$$

The numerical results are summarized in Table 12.

The transition $6^2P_{\frac{1}{2}} - 6^2P_{\frac{3}{2}}$ has been discussed as a candidate for optical rotation experiments to detect parity violation. We compare our value of the $6^2P_{\frac{1}{2}} - 6^2P_{\frac{3}{2}}$ polarization $4.17 \cdot 10^{-7}$, with that obtained from the calculation of Henley and Wilets[23]:

$$P = 4.80 \cdot 10^{-7}, \quad \text{for } \sin^2\theta_W = 0.3 \tag{89}$$

The discrepancy of 15% is largely due to the $\langle \mathcal{E}_2 \rangle$ amplitude which Henley and Wilets ignored. Once this correction is made, the two calculations agree within 2%.

Henley and Wilets used a Green's function technique with hybrid Dirac-Schroedinger wave functions; that is, relativistic wave functions are calculated for very small r and matched to non-relativistic functions at larger r. Empirical energies rather than calculated energies (which in their case differ by ∿20%) are inserted, although it is claimed that this does not change $\mathcal{E}_{PV}$ substantially. Since Henley and Wilets do not report calculations of Tℓ parameters other than $\mathcal{E}_{PV}$ ($6^2P_{1_2}$-$6^2P_{3/2}$) we cannot make an accurate comparison of their calculation with ours or with experiments.

We note in passing that in calculations[23,24] of the optical rotation of the currently investigated $^4S_{3/2}$-$^2D_{3/2}$ and $^4S_{3/2}$-$^2D_{5/2}$ transitions in bismuth, the effect of $\langle\mathcal{E}_2\rangle$ is ignored. In the calculations of Garstang[20] for these transitions, the $\mathcal{E}_2$ amplitude in $^4S_{3/2}$-$^2D_{3/2}$ is in fact negligible, but the large $\mathcal{E}_2$ amplitude calculated for $^4S_{3/2}$-$^2D_{5/2}$ would reduce the optical rotation by ∿30%. A more precise calculation may alter this result substantially.

The Tℓ transitions $6^2P_{3/2}$-$7^2P_{1/2}$, $6^2P_{1/2}$-$7^2P_{3/2}$ may also be considered in optical rotation experiments, although the experimental difficulties are formidable.

CHAPTER I REFERENCES

1. F.J. Hasert et al., Phys. Lett. 46B, 121, 138 (1973), Nucl. Phys. B73, 1 (1974).

A. Benvenuti et al., Phys. Rev. Lett. 32, 800 (1974), Phys. Rev. Lett. 37, 1039 (1976).

B. Aubert et al., Phys. Rev. Lett. 32, 1454 (1974).

S.J. Barish et al., Phys. Rev. Lett. 33, 418 (1974), Phys. Rev. Lett. 36, 179 (1976).

B.C. Barish et al., Phys. Rev. Lett. 34, 538 (1975).

W. Lee et al., Phys. Rev. Lett. 37, 186 (1976).

see Albright, C.H. et al., FERMILAB-Pub.-76/40-Thy preprint for a recent review of the high energy experimental situation.

2. S. Weinberg, Phys. Rev. Lett. 19, 1264 (1967), Phys. Rev. Lett. 27, 1688 (1971), Phys. Rev. D5, 1412 (1972).

A. Salam, in Elementary Particle Theory ed. N. Svartholm (Stockholm: Almquist and Forlag) 1968.

For a review of renormalizable gauge theories, see T.D. Lee, Phys. Rep. 9C, no. 2 (1974) and J.C. Taylor, Gauge Theories of Weak Interactions, Cambridge University Press (1976).

3. S. Chu, R. Conti and E.D. Commins, Phys. Lett. A 60A, 96 (1977).

S. Chu, Ph.D. thesis, Lawrence Berkeley Laboratory preprint LBL - 5731.

4. M.A. Bouchiat and C.C. Bouchiat, Phys. Lett. 48B, 111 (1974), Jour. de Phys. 35, 899 (1974), Jour. de Phys. 36, 493 (1975).

5. T. Tietz, J. Chem. Phys. 22, 2094 (1954).

6. M.E. Rose, Relativistic Electron Theory, J. Wiley & Sons, Inc., New York (1961). Our f and g are not the same as Rose's.

7. C. Schwartz, Phys. Rev. 97, 380 (1955), Phys. Rev. 105, 173 (1957).

8. M. Abramowitz and I.A. Stegan, Handbook of Mathematical Functions, AMS 55, Nat. B. of Stand. (1964).

9. C.M. Lederer, J.M. Hollander, and I. Perlman, Table of Isotopes,

10. V.B. Berestetskii, E.M. Lifshitz, L.P. Pitaevskii, Relativistic Quantum Theory, (Vol. 4, pt. I of Course of Theoretical Physics) Pergamon Press, London (1971).

11. A. Gallagher and A. Lurio, Phys. Rev. 136, A87 (1964).

12. E.M. Anderson, E.K. Anderson and V.F. Trusov, Opt. i Spekt. 22, 471 (861) (1967).

13. W.R. Johnson, Phys. Rev. Lett. 29, 1123 (1972).

14. M. Phillips, Phys. Rev. 88, 209 (1952).

15. G. Breit, Phys. Rev. 34, 553 (1929), Phys. Rev. 39, 616 (1932).

16. A. Abragam and J.H. Van Vleck, Phys. Rev. 92, 1448 (1953).

17. C. Schwartz, unpublished communication (1970).

18. W.E. Lamb, Jr., Phys. Rev. 60, 817 (1941).

19. T.R. Fowler, Ph.D. thesis (UCRL-18321), University of California, Berkeley (1968).

20. R.H. Garstang, J. of Research NBS-A 68, 61 (1964).

21. F. Reines et al., Phys. Rev. Lett. 37, 315 (1976).

22. O.P. Sushkov, V.V. Flambaum, and I.B. Khriplovich, JEPT Lett. 24, 502 (1976).

23. E.M. Henley and L. Wilets, Phys. Rev. A 14, 1411 (1976).

24. M. Brimicombe, C.E. Loving, and P.G.H. Sanders, J. Phys. B. Atom. Molec. Phys. 9, L237 (1976).

25. E. Fermi and E. Segre, Zeit. Phys. 82, 729 (1933).

26. G.F. Koster, Phys. Rev. 86, 148 (1952).

27. P.J. Mohr, Ann. of Phys. 88, 26 (1974).

28. M. Gyulassy, Nucl. Phys. A, A244, 497 (1975).

FIGURE CAPTIONS

Figure 1 Low-lying energy levels of the Tℓ atom (not to scale). The hyperfine structure splittings of $6^2P_{\frac{1}{2}}$, $7^2P_{\frac{1}{2}}$ states are shown. Absorption of the $6^2P_{\frac{1}{2}}$-$7^2P_{\frac{1}{2}}$ M1 photon (292.7 nm) is detected by observing fluorescence at 535 nm. accompanying decay of the $7^2P_{\frac{1}{2}}$ state.

Figure 2 Coordinate system and orientation of electric field $\vec{E}$, laser beam, and detectors as described in this paper and utilized in the experiment of Chu, Commins and Conti.

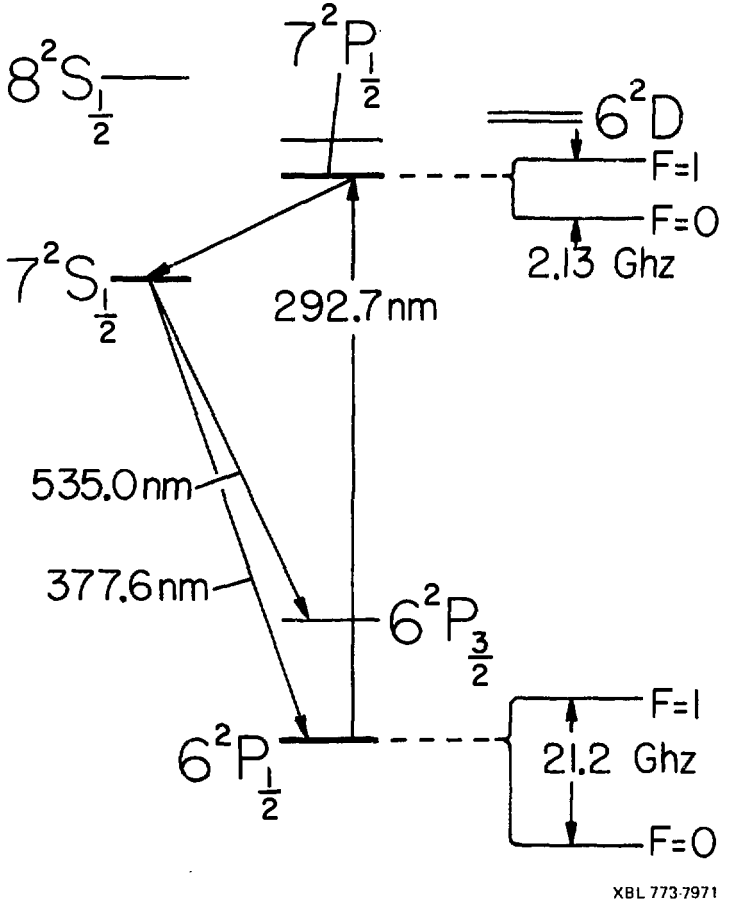
$8^2S_{\frac{1}{2}}$
$7^2P_{\frac{1}{2}}$
6^2D
F=1
F=0
2.13 Ghz
$7^2S_{\frac{1}{2}}$
292.7nm
535.0nm
377.6nm
$6^2P_{\frac{3}{2}}$
$6^2P_{\frac{1}{2}}$
F=1
21.2 Ghz
F=0
XBL 773-7971

Figure 1

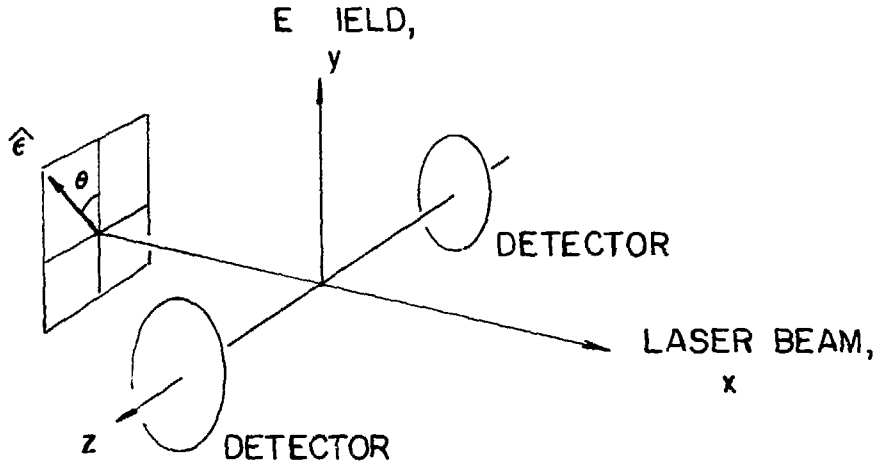

XBL 773-7970

Figure 2

APPENDIX A

Interconfiguration Interaction and Hyperfine Structure of the $6^2P_{3/2}$ State

It is well known that the observed hfs of the $6^2P_{3/2}$ state in Tl differs markedly from that calculated in the ORCF approximation using the single $5d^{10}\ 6s^2 6p_{3/2}$ configuration, because the actual atomic state contains admixtures of other configurations,[25] notably (...6s 7s 6p). We write the unperturbed wave function (...$6s^2 6_p$) as ψ_0 and form two possible $P_{3/2}$ (or $P_{\frac{1}{2}}$) states from the 6s 7s 6p configuration. These are ψ_1 (6s 7s ($^3S_1$) 6p ^2P_J) with the 2 s electrons in a spin-one state, and ψ_2 (6s 7s ($^1S_0$) 6p ^2P_J) with the total s electron spin equal to zero. The states and notation are similar to those of Koster,[26] who performs a similar calculation for gallium. We write for the total wave-function:

$$\psi = \alpha_0\psi_0 + \alpha_1\psi_1 + \alpha_2\psi_2 \tag{A1}$$

The coefficients α_1, α_2 are given in first order perturbation theory by

$$\alpha_1 = \frac{\langle\psi_1|V|\psi_0\rangle}{E_0 - E_1} \tag{A2}$$

and

$$\alpha_2 = \frac{\langle\psi_2|V|\psi_0\rangle}{E_0 - E_2} \tag{A3}$$

where $V = \sum_{i<j} \frac{e^2}{r_{ij}}$ and the matrix elements of V in A2, A3 are calculated from the electrostatic integral:

$$F_0(6s,\ 6s;\ 6s,\ 7s) = \iint \psi_{6s}(\vec{x}_1)\psi_{6s}(\vec{x}_2)\ \frac{e^2}{r_{12}}\ \psi_{6s}(\vec{x}_1)\psi_{7s}(\vec{x}_2)\ d\tau_1 d\tau_2$$

and the similar and direct exchange integrals $F_0(6s,\ 6p;\ 7s,\ 6p)$ and $G_1(6s,\ 6p;\ 6p,\ 7s)$. We use the 6s wave-function (ionization energy = $2.3376 \cdot 10^{-5}$) calculated from Eq. (4). This is not self-consistent, since that central potential already includes the $6s^2$ charge distribution. However, this introduces an error estimated at only 10 to 15% in the ionization energy. The 7s and $6p_J$ states are calculated in the same central potential, and the energy denominator is approximated by the 6S-7S energy difference. Normalizing with $\alpha_0^2 + \alpha_1^2 + \alpha_2^2 = 1$, we find:

$$\begin{aligned} 6P_{1/2}: &\quad \alpha_0 = 0.97, \quad \alpha_1 = +0.0097, \quad \alpha_2 = +0.23 \\ 6P_{3/2}: &\quad \alpha_0 = 0.97, \quad \alpha_1 = 0.029 \qquad \alpha_2 = 0.22 \end{aligned} \tag{A4}$$

The large difference $\alpha_1(P_{3/2}) - \alpha_1(P_{1/2})$ occurs because of a corresponding difference in the exchange integral G_1 (6s, 6p; 6p, 7s) between $6P_{3/2}$ and $6P_{1/2}$ states.

The hfs splitting is:

$$\begin{aligned} \Delta_{3/2} &= \Delta_0(6^2P_{3/2}) + \frac{4}{9}\alpha_1^2\ (\Delta_{6s} + \Delta_{7s}) \\ &\quad - \frac{4}{3\sqrt{3}}\alpha_1\alpha_2\ (\Delta_{6s} - \Delta_{7s}) - \frac{2}{3\sqrt{6}}\alpha_1\alpha_2\sqrt{\Delta_{6s}\ \Delta_{7s}} \\ \Delta_{1/2} &= \Delta_0(6^2P_{1/2}) + \frac{2}{9}\alpha_1^2\ (\Delta_{6s} + \Delta_{7s}) + \frac{2}{3\sqrt{3}}\alpha_1\alpha_2(\Delta_{6s} - \Delta_{7s}) \\ &\quad + \frac{4}{3\sqrt{6}}\sqrt{\Delta_{6s}\Delta_{7s}} \end{aligned} \tag{A5}$$

where only the dominating s-electron perturbation is included.

In formulae (A5) we use the experimental value of Δ_{7S}, Eq. (A4), and the calculated value Δ_{6S} = 135 Ghz. The numerical results are summarized in Table A1. They show that the $6^2P_{3/2}$ hfs is strongly affected by configuration mixing while the $6^2P_{\frac{1}{2}}$ hfs is not. Further, similar corrections can be obtained for 6snsδp configurations with n>7. That of the 6s8s6p and 6s9s6p configurations is also included in Table A1. We find for $6s8s6p_{3/2}$: $\alpha_1 = 0.012$, $\alpha_2 = 0.09$; while for $6s9s6p_{3/2}$, $\alpha_1 = 0.007$, $\alpha_2 = 0.05$.

Because of the uncertainties and lack of self-consistency inherent in the present approach, there is no profit in attempting to include contributions of configurations $6sns6p_{3/2}$ with n>9.

Table AI.

State	Unperturbed Hfs splitting: ΔE_0	Hfs splitting including (6s7s6p) correction: $\Delta E_1 = \Delta E_0 + \delta(6s7s6p)$	$\Delta E_2 = \Delta E_1 + \delta(6s8s6p) + \delta(6s9s6p)$	Observed Hfs splitting
$6^2P_{1/2}$	21.8 Ghz	22.1	22.1	21.33
$6^2P_{3/2}$	3.27 Ghz	1.37	0.81	0.518

APPENDIX B

We demonstrate that the effect of the 6s6p7p autoionizing state is taken into account (approximately) by calculating the amplitude α_{PV} if a term corresponding to the unphysical $6s^2$ 6s state is included. The term in question is:

$$T = \frac{\langle 6s6s7p|\hat{\epsilon}\cdot r|6s6p7p\rangle\langle 6s6p7p|H'_{PV}|6s6s6p\rangle}{E_{6s6s6p} - E_{6s6p7p}} + \frac{\langle 6s6s7p|H'_{PV}|6s6p7p\rangle\langle 6s6p7p|\hat{\epsilon}\cdot r|6s6s6p\rangle}{E_{6s6s7p} - E_{6s6p7p}} \quad \text{(B1)}$$

Now:

$$\langle 6s6s7p|\hat{\epsilon}\cdot\vec{r}|6s6p7p\rangle\langle 6s6p7p|H'|6s6s6p\rangle =$$
$$- \langle 6s|\hat{\epsilon}\cdot\vec{r}|6p\rangle\langle 7p|H'_{PV}|6s\rangle =$$
$$- \langle 7p|H'_{PV}|6s\rangle\langle 6s|\hat{\epsilon}\cdot\vec{r}|6p\rangle \quad \text{(B2)}$$

and

$$\langle 6s6s7p|H'_{PV}|6s6p7p\rangle\langle 6s6p7p|\hat{\epsilon}\cdot\vec{r}|6s6s6p\rangle =$$
$$- \langle 7p|\hat{\epsilon}\cdot\vec{r}|6s\rangle\langle 6s|H'_{PV}|6p\rangle \quad \text{(B3)}$$

Furthermore $E_{6s6s7p} - E_{6s6p7p} \cong -(E_{6p} - E_{6s})$ (B4)

and $E_{6s6s6p} - E_{6s6p7p} \cong -(E_{7p} - E_{6s})$ (B5)

Inserting B2 - B5 in B1 we obtain:

$$T = \frac{\langle 7p|\hat{\epsilon}\cdot\vec{r}|6s\rangle\langle 6s|H'_{PV}|6p\rangle}{E_{6p} - E_{6s}} + \frac{\langle 7p|H'_{PV}|6s\rangle\langle 6s|\hat{\epsilon}\cdot\vec{r}|6p\rangle}{E_{7} - E_{6s}} \quad \text{(B6)}$$

which is the desired result.

APPENDIX C

Construction and Use of the Dirac Green's Function

The construction of the Dirac Green's function has been described by Mohr,[27] and Gyulassy,[28] with emphasis on the case of a spherically symmetric central potential. This function is a solution of the differential equation:

$$(H(\vec{r}_2) - E)\, G(\vec{r}_1,\vec{r}_2, E) = I\delta^3(\vec{r}_2-\vec{r}_1) \tag{C1}$$

where H is the Dirac Hamiltonian with potential $V(\vec{r}_2) = V(|\vec{r}_2|)$ and I is the 4x4 identity matrix. Separation of radial and angular variables is accomplished by writing

$$G(\vec{r}_2,\vec{r}_1,E) = \sum_{\kappa,\mu}\begin{pmatrix} G^{11}_\kappa(r_2,r_1,E)\ \chi^\mu_\kappa(\vec{e}_2)\chi^{\mu\,\dagger}_\kappa(\vec{e}_1) & G^{12}_\kappa(r_2,r_1,E)\,\chi^\mu_\kappa(\vec{e}_2)\chi^{\mu\,\dagger}_{-\kappa}(\vec{e}_1) \\ iG^{21}_\kappa(r_2,r_1,E)\chi^\mu_{-\kappa}(\vec{e}_2)\chi^{\mu\,\dagger}_\kappa(\vec{e}_1) & G^{22}_\kappa(r_2,r_1,E)\chi^\mu_{-\kappa}(\vec{e}_2)\chi^{\mu\,\dagger}_{-\kappa}(\vec{e}_1)\end{pmatrix} \tag{C2}$$

where the $\chi\ (\vec{e})$ are the same functions as defined in Eq. (13). Eq. (C2) is justified by the completeness relation:

$$\sum_{\kappa,\mu}\chi^\mu_\kappa(\vec{e}_2)\chi^{\mu\,\dagger}_\kappa(\vec{e}_1) = \begin{pmatrix}1 & 0\\ 0 & 1\end{pmatrix}\delta(\phi_2-\phi_1)\delta(\cos\theta_2 - \cos\theta_1)$$

Only $G^{ij}_{\kappa=-1}$ contributes to ℓ_{PV} ($S_{\frac{1}{2}}$-states) while for ℓ (Stark mixing), the terms $G^{ij}_{\kappa=-1}$ ($S_{\frac{1}{2}}$ states) and $G^{ij}_{\kappa=2}$ ($D_{3/2}$ states) contribute. Eq. (C1) reduces to a 2x2 radial equation:

$$\begin{pmatrix} 1+V(r_2)-E & -\frac{1}{r_2}\frac{\partial}{\partial r_2}(r_2)+\frac{\kappa}{r_2} \\ \frac{1}{r_2}\frac{\partial}{\partial r_2}(r_2)+\frac{\kappa}{r_2} & -1+V(r_2)-E \end{pmatrix} \begin{pmatrix} G_\kappa^{11}(r_2,r_1,E) & G_\kappa^{12}(r_2,r_1,E) \\ G_\kappa^{21}(r_2,r_1,E) & G_\kappa^{22}(r_2,r_1,E) \end{pmatrix}$$

$$= \begin{pmatrix} 1 & 0 \\ 0 & 1 \end{pmatrix} \frac{\delta(r_2-r_1)}{r_2 r_1} \qquad \text{(C3)}$$

It can be shown that the solution of C3 is:

$$G_\kappa(r_2,r_1,E) = \frac{1}{J^\kappa(E)} \left\{ \theta(r_1-r_2) \begin{pmatrix} F_<^\kappa(r_2)F_>^\kappa(r_1) & F_<^\kappa(r_2)G_>^\kappa(r_1) \\ G_<^\kappa(r_2)F_>^\kappa(r_1) & G_<^\kappa(r_2)G_>^\kappa(r_1) \end{pmatrix} \right.$$

$$\left. + \theta(r_2-r_1) \begin{pmatrix} F_>^\kappa(r_2)F_<^\kappa(r_1) & F_>^\kappa(r_2)G_<^\kappa(r_1) \\ G_>^\kappa(r_2)F_<^\kappa(r_1) & G_>^\kappa(r_2)G_<^\kappa(r_1) \end{pmatrix} \right\} \qquad \text{(C4)}$$

where $J^\kappa(E)$ is the Wronskian:

$$J^\kappa(E) = r^2 \left\{ G_<^\kappa(r)F_>^\kappa(r) - G_>^\kappa(r)F_<^\kappa(r) \right\}$$

and F^κ, G^κ are solutions of the equation:

$$\begin{pmatrix} 1+V(r)-E & \left(-\frac{1}{r}\frac{d(r)}{dr}+\frac{\kappa}{r}\right) \\ \left(\frac{1}{r}\frac{d(r)}{dr}+\frac{\kappa}{r}\right) & -1+V(r)-E \end{pmatrix} \begin{pmatrix} F \\ G \end{pmatrix} = 0 \qquad \text{(C5)}$$

$\begin{pmatrix} F_< \\ G_< \end{pmatrix}$ is the solution which is regular as $r \to 0$, while $\begin{pmatrix} F_> \\ G_> \end{pmatrix}$ is the solution regular as $r \to \infty$. These solutions are calculated in the same manner as the

eigensolutions of Eq. (11), that is, by numerical integration of the differential equation starting with the asymptotic solution either for small r (for $F_<$, $G_<$ and using V(r) in (c) of Section 2.1) or for large r (for $F_>$, $G_>$, using $V(r) \to \frac{-e^2}{r}$). We note that F, G of (C5) correspond to f/r, g/r of Eq. (13).

The parity violating amplitude $\mathcal{E}_{PV}$ of Eq. (68) can be written as:

$$\mathcal{E}_{PV} = -\iint \langle \psi_{7^2_{p_{1/2}}}^{\mu_1}(\vec{r}_1)|e\vec{\varepsilon}\cdot\vec{r}\; G(\vec{r}_1,\vec{r}_2,E_{6p})\; H_{PV}|\psi_{6^2_{p_{1/2}}}^{\mu_2}(\vec{r}_2)\rangle d^3\vec{r}_2 d^3\vec{r}_1$$

$$-\iint \langle \psi_{7^2_{p_{1/2}}}^{\mu_1}(\vec{r}_1)|H_{PV}G(\vec{r}_1,\vec{r}_2,E_{7p})e\hat{\varepsilon}\cdot\vec{r}|\psi_{6^2_{p_{1/2}}}^{\mu_2}(\vec{r}_2)\rangle d^3\vec{r}_2 d^3\vec{r}_1 \qquad \text{(C6)}$$

Because of the short range character of H_{PV} the first term in C6 becomes:

$$-e\int_0^\infty f_{7p}\, r_2 (r_2\, F^{(\kappa=-1)}(r_2,E_6))dr_2 \cdot \int \chi_1^{m_1\dagger}\, \hat{\varepsilon}\cdot\vec{e}_r\, \chi_{-1}^{m_2} \cdot$$

$$\frac{iGQ_W}{8\pi\sqrt{2}} \cdot \frac{1}{J(E_6)R^2} \cdot \left\{ (RF_<^{(\kappa=-1)}(R,E_6)\, g_{6p}(R) - (RG_<^{(\kappa=-1)}(R,E_6))\, f_{6p}(R) \right\}_{R<r_{nuc}}$$

(C7)

In practice this expression is averaged over the region $R \le r_{nuc}$, where r_{nuc} is the nuclear radius. The second term in C6 becomes:

$$+e\int f_{6p} r_1 (r_1 F_>^{(\kappa=-1)}(r_1,E_7))\, dr_1 \cdot \chi_{-1}^{m_1\dagger}\, \hat{\varepsilon}\cdot\vec{e}_r \chi_1^{m_2} \cdot$$

$$\frac{iGQ_W}{8\pi\sqrt{2}\, J(E_7)R^2} \left\{ (RF_<^{(\kappa=-1)}(R,E_7) g_{7p}(R) - (RG_<^{(\kappa=-1)}(R,E_7)) f_7(R) \right\}$$

(C8)

A similar calculation was performed for $\mathcal{E}_S$ (Sec. 5). In this case only "large" components (f,F) contribute significantly. For example, the matrix element α of Eq. (82) is written:

$$\alpha = -\frac{1}{9}\left[\int_0^\infty\int_0^\infty \frac{f_{7p}(r_2)r_2(r_<F_<^{(\kappa=-1)}(r_<,E_6))(r_>F_>^{(\kappa=-1)}(r_>,E_6))r_1 f_{6p}(r_1)dr_1dr_2}{J(E_6)}\right.$$

$$\left.+\int_0^\infty\int_0^\infty \frac{f_{7p}(r_2)r_2(r_<F_<^{(\kappa=-1)}(r_<,E_7))(r_>F_>^{(\kappa=-1)}(r_>, \quad))r_1 f_{6p}(r_1)dr_1dr_2}{J(E_7)}\right]$$

$$-\frac{2}{9}\cdot\left[\text{same as above with } \kappa = +2\right] \qquad \text{(C9)}$$

In all of the above expressions,

$r_>$ = larger of r_1, r_2

$r_<$ = smaller of r_1, r_2.

The expression for β (Eq. 83) is obtained in the same way.

Table I. Dirac radial functions f/r, g/r for selected states.

r (ft)	$6P_{3/2}$ f(r)/r	$6P_{3/2}$ g(r)/r	$6P_{3/2}$ f(r)/r	$6P_{3/2}$ g(r)/r	$7P_{1/2}$ f(r)/r	$7P_{1/2}$ g(r)/r	$7S_{1/2}$ f(r)/r	$7S_{1/2}$ g(r)/r	$6D_{3/2}$ f(r)/r	$6D_{3/2}$ g(r)/r
.02	2.383×10^{-3}	5.985×10^{-3}	4.014×10^{-5}	-4.454×10^{-6}	8.391×10^{-4}	2.107×10^{-3}	8.491×10^{-3}	-2.090×10^{-3}	1.582×10^{-7}	1.329×10^{-6}
.12	1.678	3.970	2.004×10^{-4}	-3.040×10^{-5}	5.908	1.398	5.782	-1.915	1.339×10^{-6}	6.675×10^{-6}
.32	1.739	3.000	4.608	-7.035	6.122	1.056	4.146	-1.459	4.416	1.555×10^{-5}
.62	1.920	2.300	7.678	-1.184×10^{-4}	6.761	8.101×10^{-4}	2.889	-1.111	1.088×10^{-5}	2.645
1.42	2.177	1.329	1.272×10^{-3}	-2.022	7.667	4.146	1.837	-6.232×10^{-4}	3.568	4.641
2.40	2.116	7.010×10^{-4}	1.491	-2.483	7.452	2.469	1.178×10^{-4}	-3.113	7.335	5.913
4.40	1.458	1.170	1.272	-2.431	5.492	4.119×10^{-5}	-5.184	-3.300	1.479×10^{-4}	6.307
6.40	6.498×10^{-4}	-7.624×10^{-5}	7.541×10^{-4}	-1.862	2.288	-2.686	-4.468	4.905×10^{-5}	1.968	5.373
8.40	3.484×10^{-5}	-1.181×10^{-4}	2.579	-1.223	1.221×10^{-5}	-4.159	-2.095	5.933	2.212	4.072
10.40	-3.545×10^{-4}	-1.029	-1.120	-6.774×10^{-5}	-1.249×10^{-4}	-5.623	8.735×10^{-6}	4.549	2.192	2.812
12.40	-5.474	-7.090×10^{-5}	-3.412	-2.690	-1.928	-2.496	1.557×10^{-4}	2.674	1.999	1.748
14.40	-5.949	-3.882	-4.501	8.953×10^{-7}	-2.045	-1.366	2.296	1.035	1.698	9.173×10^{-6}
18.40	-4.428	6.076×10^{-6}	-4.693	1.802×10^{-5}	-1.559	2.152×10^{-6}	2.224	-9.259×10^{-6}	9.727×10^{-5}	-1.242
24.00	-7.630×10^{-5}	2.738×10^{-5}	-1.759	2.833	-2.673×10^{-5}	9.650	7.174×10^{-5}	-1.448×10^{-5}	5.380×10^{-6}	-6.513
44.00	2.924×10^{-4}	5.932×10^{-7}	2.646	-4.910×10^{-6}	1.028×10^{-4}	1.943×10^{-7}	-1.331×10^{-4}	2.688×10^{-6}	-8.549×10^{-5}	-2.090
64.00	-2.830×10^{-5}	-7.414×10^{-6}	4.584×10^{-5}	-6.436	-1.058×10^{-5}	-2.617×10^{-6}	2.078×10^{-5}	3.321	-2.523	1.021
84.00	-2.000×10^{-4}	-4.208	-1.308×10^{-4}	-1.843	-7.059	-1.472	9.622	5.844×10^{-7}	2.586	1.371
120.00	-1.161	4.658×10^{-7}	-1.616	1.631	-5.575	1.881×10^{-7}	5.576	-1.094×10^{-6}	5.549	7.503×10^{-7}
220.00	1.172	1.125×10^{-6}	6.475×10^{-5}	5.257×10^{-7}	4.251	3.866	-6.797	-8.433×10^{-8}	2.296	-2.148×10^{-8}
320.00	1.497	3.751×10^{-7}	1.230×10^{-4}	-1.560	4.866	8.494×10^{-8}	-4.468	2.076×10^{-7}	-5.243×10^{-6}	-1.241×10^{-7}
420.00	1.174	9.062×10^{-8}	1.107	-2.489	2.984	-3.331	-5.083×10^{-6}	1.712	-1.971×10^{-5}	-1.211
620.00	5.470×10^{-5}	-4.168	6.172×10^{-5}	-1.546	-5.002×10^{-6}	-7.184	3.604×10^{-5}	4.523×10^{-8}	-3.048	-8.423×10^{-8}
820.00	2.313	-2.271	3.007	-7.456×10^{-8}	-2.191×10^{-5}	-5.060	4.121	-9.513×10^{-9}	-3.144	-5.262
1020.00	9.481×10^{-6}	-1.205	1.400	-5.061	-2.651	-2.763	3.375	-2.372×10^{-8}	-2.804	-3.074
1420.00	1.531	-2.444×10^{-9}	2.852×10^{-6}	-6.770×10^{-9}	-2.074	-3.184×10^{-9}	1.617	-1.735	-1.865	-8.203×10^{-9}
1820.00	2.402×10^{-7}	-4.271×10^{-10}	3.188×10^{-7}	-1.300	-1.203	2.811	6.387×10^{-6}	-7.867×10^{-9}	-1.075	-7.861×10^{-10}
2600.00	6.195×10^{-8}	-1.224×10^{-11}	2.155×10^{-8}	-4.915×10^{-11}	-2.960×10^{-6}	1.777	8.224×10^{-7}	-1.131	-2.953×10^{-6}	9.397
3100.00	5.710×10^{-10}	-1.219×10^{-12}	3.197×10^{-9}	-4.917×10^{-12}	-1.067	7.784×10^{-10}	2.025	-2.884×10^{-10}	-1.160	5.451
3600.00					-3.634×10^{-7}	2.984	4.788×10^{-8}	-6.975×10^{-12}	-4.377×10^{-7}	2.529
4100.00					-1.189	1.058	1.109	-1.617	-1.593	1.051
4600.00					-3.776×10^{-8}	3.563×10^{-11}	2.825×10^{-9}	-3.256×10^{-12}	-5.638×10^{-8}	4.083×10^{-11}
5600.00					-3.316×10^{-9}	3.946×10^{-12}			-6.639×10^{-9}	5.435×10^{-12}
6600.00									-7.359×10^{-10}	6.509×10^{-13}

Table II.

Spectroscopic level designation	Fitted energy level (ionization energy, $m_e c^2=1$)	Spectroscopic energy level[a]	Valence-electron hyperfine splitting (GHz)	Observed hyperfine splitting (GHz)
$6p\,^2P_{1/2}$	1.1939×10^{-5}	1.1953×10^{-5}	21.8	21.3[b]
$6p\,^2P_{3/2}$	9.8745×10^{-6}	1.0062×10^{-5}	3.27	.528[c]
$7p\,^2P_{1/2}$	3.6756×10^{-6}	3.6648×10^{-6}	2.71	2.13[d]
$7p\,^2P_{3/2}$	3.3937×10^{-6}	3.4219×10^{-6}	.494	.62[d]
$8p\,^2P_{1/2}$	1.9199×10^{-6}	1.9158×10^{-6}	.989	.79[e]
$8p\,^2P_{3/2}$	1.8155×10^{-6}	1.8254×10^{-6}	.187	.26[e]
$7s\,^2S_{1/2}$	5.4164×10^{-6}	5.5289×10^{-6}	14.3	12.4[b]
$8s\,^2S_{1/2}$	2.5169×10^{-6}	2.5521×10^{-6}	4.32	
$9s\,^2S_{1/2}$	1.4650×10^{-6}	1.4796×10^{-6}	1.90	
$10s\,^2S_{1/2}$	9.594×10^{-7}	9.6260×10^{-7}	1.01	
$11s\,^2S_{1/2}$	6.772×10^{-7}	6.811×10^{-7}	0.59	

Table II References.

a) C.E. Moore, Atomic Energy Levels Vol. III, Circular of Nat. B. of Stand. 467 (1958).

b) A. Gallagher and A. Lurio, Phys. Rev. 136, A87 (1964).

c) G. Gould, Phys. Rev. 101, 1828 (1956).

d) A. Flusberg, T. Mossberg and S.R. Hartmann, Phys. Lett. 55A, 403 (1976).

e) A.N. Odintsov, Opt. i Spektr. 9, 75 (142), (1960).

Table III.

Transition	A-coefficient (Gallagher & Lurio)[a] 10^7 sec^{-1}	A-coefficient (this work) 10^7 sec^{-1}	Radial integral $\langle r \rangle_{fi}$ (Å)	Oscillator strength (this work)	Oscillator strength (A,A,&T)[b]
$7^2S_{1/2}$-$6^2P_{1/2}$	6.25±0.31	5.78	294.1	.124	.123
$8^2S_{1/2}$-$6^2P_{1/2}$	1.78±0.16	1.75	91.5	.0175	.0172
$9^2S_{1/2}$-$6^2P_{1/2}$	.78±0.10	0.777	51.8	.00625	.00616
$10^2S_{1/2}$-$6^2P_{1/2}$	---	0.412	35.1	.00301	.00295
$11^2S_{1/2}$-$6^2P_{1/2}$	.31±0.06	0.244	26.0	.00170	.00167
$7^2S_{1/2}$-$6^2P_{3/2}$	7.05±0.32	8.30	422.1	.178	.162
$8^2S_{1/2}$-$6^2P_{3/2}$	1.73±0.18	2.30	103.9	.0180	.0172
$9^2S_{1/2}$-$6^2P_{3/2}$	0.80±0.08	1.01	56.3	.00605	.0059
$10^2S_{1/2}$-$6^2P_{3/2}$	0.57±0.06	.534	37.5	.00285	.00286
$6^2D_{3/2}$-$6^2P_{1/2}$	12.6 ±1.0	16.04	-307.7	.368	.40
$7^2D_{3/2}$-$6^2P_{1/2}$	4.4 ±0.5	6.39	-154.8	.109	.121
$8^2D_{3/2}$-$6^2P_{1/2}$	1.89±0.3	3.19	- 99.8	.0434	.053
$9^2D_{3/2}$-$6^2P_{1/2}$	.98±0.22	1.82	- 71.9	.0257	.028
$10^2D_{3/2}$-$6^2P_{1/2}$	.58±0.15	1.14	- 55.2	.0156	.017
$6^2D_{3/2}$-$6^2P_{3/2}$	2.20±0.23	2.88	-419.6	.0538	.052
$7^2D_{3/2}$-$6^2P_{3/2}$	0.76±0.08	1.01	-186.9	.0129	.0136
$8^2D_{3/2}$-$6^2P_{3/2}$	0.37±0.04	0.498	-117.5	.00549	.0056
$9^2D_{3/2}$-$6^2P_{3/2}$	0.19±0.02	0.279	- 83.0	.00285	.0029
$6^2D_{5/2}$-$6^2P_{3/2}$	12.4 ±1.5	16.3	-405.6	.489	.46
$7^2D_{5/2}$-$6^2P_{3/2}$	4.2 ±0.5	6.06	-186.9	.116	.12
$8^2D_{5/2}$-$6^2P_{3/2}$	1.7 ±0.2	2.96	-116.9	.0489	.051

[a] Ref. 11

[b] Ref. 12

Table IV.

Transition	Radial integral <r>pi (Å)	Oscillator strength (this work)	Oscillator strength[12] (A,A & T)
$7^2S_{1/2}$-$7^2P_{1/2}$	-1072.6	.315	.440
$8^2S_{1/2}$-$7^2P_{1/2}$	991.6	.241	.258
$9^2S_{1/2}$-$7^2P_{1/2}$	219.5	.0234	.0219
$10^2S_{1/2}$-$7^2P_{1/2}$	114.3	.00784	.00741
$11^2S_{1/2}$-$7^2P_{1/2}$	75.1	.00277	.00342
$7^2S_{1/2}$-$7^2P_{3/2}$	-1007.8	.476	.440
$8^2P_{1/2}$-$7^2P_{3/2}$	1240.2	.297	.294
$9^2S_{1/2}$-$7^2P_{3/2}$	202.2	.0176	.0164
$10^2S_{1/2}$-$7^2P_{3/2}$	100.4	.00550	.00542
$6^2D_{3/2}$-$7^2P_{1/2}$	1321.4	.369	.340
$7^2D_{3/2}$-$7^2P_{1/2}$	- 489.2	.202	.248
$8^2D_{3/2}$-$7^2P_{1/2}$	- 254.2	.0733	.0850
$9^2D_{3/2}$-$7^2P_{1/2}$	- 165.3	.0352	.0399
$10^2D_{3/2}$-$7^2P_{1/2}$	- 120.0	.0199	.0223
$6^2D_{3/2}$-$7^2P_{3/2}$	1328.0	.0152	.0166
$7^2P_{3/2}$-$7^2P_{3/2}$	- 729.8	.0396	.0418
$8^2D_{3/2}$-$7^2P_{3/2}$	- 331.0	.00937	.0116
$9^2D_{3/2}$-$7^2P_{3/2}$	- 204.9	.00495	.00506

Table V. g-factor anomaly calculation and comparison with experiment.

Measured $6^2P_{\frac{1}{2}}$ g-factor	0.6656924 (18)[a]
0-order theory	0.6658936
g-factor anomaly	-0.0002012 (18)[a]
calculated anomaly	
relativistic	-0.000107
configuration interaction	<0.000001
lamb	-0.000006
orbit-orbit	-0.000082
Total calculated anomaly	-0.000195

[a]Ref. 19.

Table VI

Transition	$m \times 3/\sqrt{2}$	$A_{m1}(\text{sec}^{-1})$	$\int_0^\infty f_f r^2 f_i dr$, (Å^2)	$A_{E2}(\text{sec}^{-1})$
$6^2P_{1/2} - 6^2P_{3/2}$	+0.9796	4.083	$2.94 \cdot 10^5$	0.158
$6^2P_{1/2} - 7^2P_{3/2}$	-0.0902	3.31	$-1.27 \cdot 10^5$	55.2
$7^2P_{1/2} - 6^2P_{3/2}$	-0.115	2.18	$-3.00 \cdot 10^5$	72.8
$7^2P_{1/2} - 7^2P_{3/2}$	+0.9822	$8.706 \cdot 10^{-3}$	$2.40 \cdot 10^6$	$3.69 \cdot 10^{-4}$

Table VII. Calculation of δ_{PV}

Method A:

Intermediate s-state	Contributions to δ_{PV}: $\frac{\langle 7P_{\frac{1}{2}}\|E1\|ns\rangle\langle ns\|H_{PV}\|6P_{\frac{1}{2}}\rangle}{E_6 - E_n}$	$\frac{\langle 7P_{\frac{1}{2}}\|H_{PV}\|ns\rangle\langle ns\|E1\|6P_{\frac{1}{2}}\rangle}{E_7 - E_n}$
$\|6s\rangle$	$-i\ 0.197 \cdot 10^{-10} Q_w\|\mu_B\|$	$+i\ 0.631 \cdot 10^{-10} Q_w\|\mu_B\|$
$\|7s\rangle$	$+i\ 5.08$	$-i\ 1.69$
$\|8s\rangle$	$-i\ 1.77$	$+i\ 0.485$
$\|9s\rangle$	$-i\ 0.232$	$+i\ 0.093$
$\|10s\rangle$	$-i\ 0.084$	$+i\ 0.037$
Total	$i\ 2.81 \cdot 10^{-10} Q_w\|\mu_B\|$	$-i\ 0.45 \cdot 10^{-10} Q_w\|\mu_B\|$
	$= i\ 2.36 \cdot 10^{-10} Q_w\|\mu_B\|$	
Method B:	$i\ 2.13 \cdot 10^{10} Q_w\|\mu_B\|$	$-i\ 0.20 \cdot 10^{-10} Q_w\|\mu_B\|$
	$= i\ 1.93 \cdot 10^{-10} Q_w\|\mu_B\|$	

Table VIII. $\mathcal{E}_{PV}$ for $n'P_{1/2}$ - $nP_{3/2}$ transitions.

Method 1: $\sum \dfrac{e\langle nP_{3/2}|E1|ns\rangle\langle ns|H_{PV}|n'P_{1/2}\rangle}{E_{P_{1/2}} - E_S}$

Intermediate s-state	$6^2P_{3/2}$-$6^2P_{1/2}$	$7^2P_{3/2}$-$6^2P_{1/2}$	$6^2P_{3/2}$-$7^2P_{1/2}$
|6s>	$-i\ 4.22 \times 10^{-10} Q_w \lvert\mu_B\rvert$	-i 0.65	-i 0.86
|7s>	-i 2.83	+i 6.76	+i 3.43
|8s>	-i 0.264	-i 3.13	-i 0.78
|9s>	-i 0.041	-i 0.30	-i 0.14
|10s>	-i 0.041	-i 0.10	-i 0.06
Total	$-i\ 7.45 \times 10^{-10} Q_w \lvert\mu_B\rvert$	+i 2.58	+i 1.58
Method 2:	$-i\ 8.09 \times 10^{-10} Q_w \lvert\mu_B\rvert$	$+i\ 1.75 \times 10^{-10} Q_w \lvert\mu_B\rvert$	$+i\ 1.25 \times 10^{-10} Q_w \lvert\mu_B\rvert$

Table IX

Quantity Summed	Finite sum over 5 lowest energy levels ($7^2S_{1/2}$ - $11^2S_{1/2}$, $6^2D_{3/2}$ - $10^2D_{3/2}$)	Green's function method
$\frac{R_{7P,nS}\, R_{nS,6P}}{E_6 - E_{nS}}$	$3.78 \cdot 10^{10}$	$3.64 \cdot 10^{10}$
$\frac{R_{7P,nS}\, R_{nS,6P}}{E_7 - E_{nS}}$	$-2.58 \cdot 10^{11}$	$-2.71 \cdot 10^{11}$
$\frac{R_{7P,nD}\, R_{nD,6P}}{E_6 - E_{nD}}$	$3.50 \cdot 10^{10}$	$2.81 \cdot 10^{10}$
$\frac{R_{7P,nD}\, R_{nD,6P}}{E_7 - E_{nD}}$	$8.00 \cdot 10^{11}$	$7.01 \cdot 10^{11}$
$e^2\alpha$ (in units $\frac{\mu_B}{\text{volts/cm}}$)	$2.43 \cdot 10^{-5}$	$2.05 \cdot 10^{-5}$
$e^2\beta$	$1.78 \cdot 10^{-5}$	$1.64 \cdot 10^{-5}$
β/α	0.73	0.80

Table X. Dipole transition amplitudes $D = \langle M1 \rangle + \langle El_{PV} \rangle + \langle El_{STARK} \rangle$ for $6^2P_{\frac{1}{2}}$ $(F, m_F) \rightarrow 7^2P_{\frac{1}{2}}$ $(F', m_{F'})$ transitions.

$7^2P_{\frac{1}{2}}, F', m_{F'}$	$6^2P_{\frac{1}{2}}$, F 0 / m_F 0	1 / -1	1 / 0	1 / 1
0 0	$\alpha'\cos\theta$	$\frac{i}{\sqrt{2}}(\mathcal{M}\sin\theta - \beta'\sin\theta + \mathcal{E}_{PV}\cos\theta)$	$\mathcal{M}\cos\theta + \mathcal{E}_{PV}\sin\theta$	$\frac{i}{\sqrt{2}}(\mathcal{M}\sin\theta + \beta'\sin\theta + \mathcal{E}_{PV}\cos\theta)$
1 -1	$\frac{i}{\sqrt{2}}(-\mathcal{M}\sin\theta - \beta'\sin\theta - \mathcal{E}_{PV}\cos\theta)$	$\alpha'\cos\theta - \mathcal{M}\cos\theta + \mathcal{E}_{PV}\sin\theta$	$\frac{-i}{\sqrt{2}}(\mathcal{M}\sin\theta + \beta'\sin\theta + \mathcal{E}_{PV}\cos\theta)$	0
1 0	$-\mathcal{M}\cos\theta$	$\frac{i}{2}(\mathcal{M}\sin\theta - \beta'\sin\theta + \mathcal{E}_{PV}\cos\theta)$	$\alpha'\cos\theta$	$\frac{-i}{2}(\mathcal{M}\sin\theta + \beta'\sin\theta + \mathcal{E}_{PV}\cos\theta)$
1 1	$\frac{i}{\sqrt{2}}(-\mathcal{M}\sin\theta + \beta'\sin\theta - \mathcal{E}_{PV}\cos\theta)$	0	$\frac{i}{\sqrt{2}}(\mathcal{M}\sin\theta - \beta'\sin\theta + \mathcal{E}_{PV}\cos\theta)$	$\alpha'\cos\theta + \mathcal{M}\cos\theta - \mathcal{E}_{PV}\sin\theta$

$\alpha' = e^2 E_0 \alpha$ $\qquad$ $\beta' = e^2 E_0 \beta$

Table XI. $P_{3/2} - P_{1/2}$ transition amplitudes.

$m_{P_{3/2}}$ \ m_T	$\frac{1}{2}$	$-\frac{1}{2}$
$\frac{3}{2}$	$\left(\frac{\sqrt{3}\,\mathcal{H}}{2} + \frac{\mathcal{E}_2}{\sqrt{6}}\right) i \sin\theta + i\,\frac{\sqrt{3}}{2}\,\mathcal{E}_{PV}\cos\theta$	$-\sqrt{\frac{2}{3}}\,\mathcal{E}_2\cos\theta$
$\frac{1}{2}$	$-\mathcal{H}\cos\theta + \mathcal{E}_{PV}\sin\theta$	$\left(\frac{\mathcal{H}}{2} - \frac{\mathcal{E}_2}{\sqrt{2}}\right) i \sin\theta + i\,\frac{\mathcal{E}_{PV}}{2}\cos\theta$
$-\frac{1}{2}$	$\left(\frac{\mathcal{H}}{2} - \frac{\mathcal{E}_2}{\sqrt{2}}\right) i \sin\theta + i\,\frac{\mathcal{E}_{PV}}{2}\cos\theta$	$-\mathcal{H}\cos\theta + \mathcal{E}_{PV}\sin\theta$
$-\frac{3}{2}$	$-\sqrt{\frac{2}{3}}\,\mathcal{E}_2\cos\theta$	$\left(\frac{\sqrt{3}\,\mathcal{H}}{2} + \frac{\mathcal{E}_2}{\sqrt{6}}\right) i \sin\theta + i\,\frac{\sqrt{3}}{2}\,\mathcal{E}_{PV}\cos\theta$

Table XII. Amplitudes for $P_{3/2}$-$P_{1/2}$ transitions.

Transition amplitude	$6P_{3/2}$-$6P_{1/2}$	$7P_{3/2}$-$7P_{1/2}$	$6P_{3/2}$-$7P_{1/2}$
	$.98\frac{\sqrt{2}}{3}$	$-.092\frac{\sqrt{2}}{3}$	$-.115\frac{\sqrt{2}}{3}$
$\mathcal{E}_2$	.22	-.434	.767
$\mathcal{E}_{PV}$	$-i\ 8.09\times10^{-10}Q_W$	$+i\ 1.75\times10^{-10}Q_W$	$+i\ 1.26\times10^{-10}Q_W$
$P(Q_W=-140)$	4.17×10^{-7}	1.67×10^{-8}	4.85×10^{-9}

$$\mathcal{M} = \frac{-\sqrt{2}}{\omega} \int (f_{1/2}\, g_{3/2} + g_{1/2}\, f_{3/2})\, g_1(\omega r)\, dr \qquad |\mu_B|$$

$$\mathcal{E}_2 = \frac{2\omega}{5} \int f_{1/2}\, f_{3/2}\, r^2\, dr \qquad |\mu_B|$$

$$\mathcal{E}_{PV} = \frac{2\sqrt{2}}{3} \sum \frac{\langle P_{3/2}|r|ns\rangle\langle ns|H_{PV}|P_{1/2}\rangle}{E_{1/2} - E_n} \qquad |\mu_B|$$

II. CALCULATIONS OF PARITY VIOLATION IN FORBIDDEN M1 TRANSITIONS IN CESIUM

1. INTRODUCTION

Existence of a neutral, weak, parity-violating electron-nucleon interaction implies that forbidden M1 transitions in heavy atoms, e.g., $6^2P_{\frac{1}{2}}$-$7^2P_{\frac{1}{2}}$ in thallium (Tl) and $6^2S_{\frac{1}{2}}$-$7^2S_{\frac{1}{2}}$, $6^2S_{\frac{1}{2}}$-$8^2S_{\frac{1}{2}}$ in cesium (Cs) should exhibit circular dichroism. In a previous paper[1] (hereafter referred to as I) we presented calculations of the atomic properties of Tl relevant to the interpretation of observations of circular dichroism in the thallium transition in terms of the Weinberg-Salam gauge field model. Here we present analogous calculations for the Cs transitions. In both cases experiments are currently underway to detect the parity violating effect.

Our approach is the one electron central field (OECF) approximation. We find numerical solutions to the Dirac equation for the valence electron in a "Tietz" central potential:[2]

$$V(r) = -\frac{e^2(Z-1)}{r(1+\eta r)^2} - \frac{e^2}{r} \qquad (1)$$

where parameter η is chosen to give agreement between the observed and calculated $6^2S_{\frac{1}{2}}$ energies. The wave-functions obtained are used to calculate fine and hyperfine structure splittings, and allowed (E1) transition rates and excited state lifetimes. These are compared with experimental results (see Section 2). The $6^2S_{\frac{1}{2}}$-$7^2S_{\frac{1}{2}}$, $6^2S_{\frac{1}{2}}$-$8^2S_{\frac{1}{2}}$ M1 amplitudes and corrections to $g_J(6^2S_{\frac{1}{2}})$ are calculated in Section 3 and compared with experiment. Relativistic contributions to the matrix elements, as well as the "Lamb" correction and corrections due to interconfiguration interaction and hyperfine mixing are included. We find that the current theoretical formulation for these latter small effects is not entirely adequate. In Section 4, we present calculations of the parity-violating E1 amplitudes

$\mathcal{E}_{PV}(6^2S_{1/2}\text{-}7^2S_{1/2})$, $\mathcal{E}_{PV}(6^2S_{1/2}\text{-}8^2S_{1/2})$ based on the Weinberg-Salam model.[3] We find

$$\mathcal{E}_{PV}(6S - 7S) = 3.50i \times 10^{-11} \; Q_W|\mu_B| \tag{2}$$

and

$$\mathcal{E}_{PV}(6S - 8S) = 1.48i \times 10^{-11} \; Q_W|\mu_B| \tag{3}$$

Here $|\mu_B| = |e\hbar/2m_e c|$ and $Q_W = (1 - 4\sin^2\theta_W)Z\text{-}N$, where θ_W is the "Weinberg" angle. Results (2) and (3) are somewhat smaller than earlier estimates by Bouchiat and Bouchiat[4] (see Section 4). Finally, in Section 5 we calculate Stark matrix elements for the transitions $6^2S_{1/2}\text{-}7^2S_{1/2}$ in an external electric field, and compare our results to earlier calculations by Bouchiat and Bouchiat,[4] and to the experimental results of Bouchiat and Pottier.[5]

2. CESIUM WAVE FUNCTIONS IN THE ONE-ELECTRON CENTRAL FIELD APPROXIMATION

2.1. Construction of Electronic Wave-Functions

As in I, we solve the Dirac equation for the valence electron in a centrally symmetric potential V(r). The latter approximates the nucleus and 54 core electrons as a fixed charge distribution. With

$$\psi = \begin{pmatrix} \frac{f(r)}{r} & \chi^{\mu}_{\kappa}(\theta,\phi) \\ i\,\frac{g(r)}{r} & \chi^{\mu}_{-\kappa}(\theta,\phi) \end{pmatrix}, \text{ the Dirac equation}$$

reduces to the coupled radial equations:

$$\left.\begin{aligned} \frac{df}{dr} &= -\frac{\kappa}{r} f + [2 - E - V(r)]g \\ \frac{dg}{dr} &= [E + V(r)]f + \frac{\kappa}{r} g \end{aligned}\right\} \tag{4}$$

Our units are $\hbar = m_e = c = 1$, E is the ionization energy, and other notation is defined in I. The parameter η of the potential of Eq. (1) is found to be

$$\eta = 355.12\ \text{Å}^{-1} = 2.5914\ a_o^{-1} \tag{5}$$

by requiring agreement between observed and calculated $6^2S_{\frac{1}{2}}$ energies. The wave-functions are calculated by integrating Eqs. (4) stepwise from the nuclear radius $R_o = .016$Å as described in detail in I. Table 1 presents calculated $S_{\frac{1}{2}}$, $P_{\frac{1}{2}}$, $P_{\frac{3}{2}}$ energies along with the observed values (obtained from the tables of C. E. Moore[6]).

2.2. Hyperfine Splittings

In first order perturbation theory the hyperfine energy is given by:[7]

$$W_F = \frac{8\kappa}{4\kappa^2 - 1}\, eg_N\mu_N[F(F+1) - I(I+1) - J(J+1)]\int_0^\infty \frac{f(r)g(r)dr}{r^2} \tag{6}$$

For Cs^{133} (the only stable isotope), $I = 7/2$, $g_N = 5.16$,[8] leading to $F = 4,3$ for $J = 1/2$ states and $F = 5,4,3,2$ for $J = 3/2$ states. Hyperfine splittings ΔE are calculated between the highest and lowest F levels. These are related to the usual hfs interaction constants A by $\Delta E_{J=1/2} = 4A_{1/2}$ and $\Delta E_{J=3/2} = 12A_{3/2}$. The results are presented in Table 1, and compared with experimental values. Agreement is reasonably good.

2.3. Allowed E1 Transition Rates

For $P_{\frac{1}{2}}$-$S_{\frac{1}{2}}$ and $P_{\frac{3}{2}}$-$S_{\frac{1}{2}}$ E1 transitions the Einstein A coefficient is

$$A = \frac{4}{9} e^2\omega^3\ |\langle P_J|r|S_{\frac{1}{2}}\rangle|^2 \tag{7}$$

In Table 2 we present radial integrals and transition rates for $P_{\frac{1}{2}}$-$S_{\frac{1}{2}}$,

TABLE 1

State	Ionization energy (calculated) ($m_e c^2 = 1$)	Ionization energy (measured)[6]	Hyperfine energy splitting (calculated) GHz	Hyperfine energy splitting (observed) GHz
$6S_{1/2}$	7.62024×10^{-6}	7.62024×10^{-6}	9.212	$9.193 \pm <.001$[c]
$7S_{1/2}$	3.1232×10^{-6}	3.1229×10^{-6}	2.346	$2.185 \pm .012$[e]
$8S_{1/2}$	1.7201×10^{-6}	1.7117×10^{-6}	0.935	$0.876 \pm .006$[e]
$9S_{1/2}$	1.0839×10^{-6}	1.0909×10^{-6}	0.468	$0.438 \pm .008$[e]
$6P_{1/2}$	4.9081×10^{-6}	4.9622×10^{-6}	1.642	$1.168 \pm <.001$[c]
$6P_{3/2}$	4.7732×10^{-6}	4.7713×10^{-6}	0.723	$0.611 \pm .006$[b]
$7P_{1/2}$	2.3392×10^{-6}	2.3301×10^{-6}	0.498	$0.377 \pm <.001$[f]
$7P_{3/2}$	2.2953×10^{-6}	2.2715×10^{-6}	0.224	$0.199 \pm .001$[b]
$8P_{1/2}$	1.3824×10^{-6}	1.3711×10^{-6}	0.220	
$8P_{3/2}$	1.3624×10^{-6}	1.3450×10^{-6}	0.100	$0.0916 \pm .0002$[a]
$9P_{1/2}$	0.9146×10^{-6}	0.9064×10^{-6}	0.117	0.093[d]
$9P_{3/2}$	0.9037×10^{-6}	0.8924×10^{-6}	0.054	

[a] H. Bucka and G. von Oppen, Ann. Phys. 10, 119 (1962).

[b] K. M. Kallas, G. Markova, G. Khvotenko, M. Chaika, Optik y Spek. 19, 173 (303)(1965).

[c] J. Abele, M. Baumann, W. Hartmann, Phys. Lett. A 49A, 205 (1974).

[d] P. Tsekaris, J. Farley, R. Gupta, Fifth International Conf. on Atomic Physics, Abstract J13, 250 (1976).

[e] R. Gupta, W. Happer, L. K. Lam, and S. Svanberg, Phys. Rev. A8, 2792 (1973).

[f] D. Feiertag, A. Sahm, and G. Zu Putlitz, Z. Physik 255, 93 (1972).

TABLE 2. A-coefficients in Cs

Transition	$\langle r \rangle_{fi}$ radial integral (Å)	A-coefficient (10^6 sec^{-1})
$6P_{1/2}$-$6S_{1/2}$	-861.4	37.3
$7P_{1/2}$-$6S_{1/2}$	- 80.4	2.40
$8P_{1/2}$-$6S_{1/2}$	- 30.8	0.582
$9P_{1/2}$-$6S_{1/2}$	- 18.0	0.245
$6P_{3/2}$-$6S_{1/2}$	-846.8	41.82
$7P_{3/2}$-$6S_{1/2}$	-104.0	4.11
$8P_{3/2}$-$6S_{1/2}$	- 46.6	1.34
$9P_{3/2}$-$6S_{1/2}$	- 28.6	0.623
$6P_{1/2}$-$7S_{1/2}$	747.3	8.00
$7P_{1/2}$-$7S_{1/2}$	-1777.3	3.83
$8P_{1/2}$-$7S_{1/2}$	-181.8	4.39
$9P_{1/2}$-$7S_{1/2}$	- 73.9	0.148
$6P_{3/2}$-$7S_{1/2}$	830.3	7.80
$7P_{3/2}$-$7S_{1/2}$	-1730.0	4.27
$8P_{3/2}$-$7S_{1/2}$	-230.3	0.729
$9P_{3/2}$-$7S_{1/2}$	-101.9	0.286
$6P_{1/2}$-$8S_{1/2}$	184.8	2.79
$6P_{1/2}$-$8S_{1/2}$	1605.4	1.54
$8P_{1/2}$-$8S_{1/2}$	-3016.4	0.883
$9P_{1/2}$-$8S_{1/2}$	-327.8	0.137
$6P_{3/2}$-$8S_{1/2}$	186.8	2.50
$7P_{3/2}$-$8S_{1/2}$	1750.9	1.47
$8P_{3/2}$-$8S_{1/2}$	-2919.4	0.983
$9P_{3/2}$-$8S_{1/2}$	-396.6	0.217

$P_{3/2}$-$S_{1/2}$ transitions. These numerical values are required for computation of $\mathcal{E}_{PV}$ and Stark amplitudes (Sections 4 and 5).

To judge the accuracy of these transition rates, we calculate values of Cs excited state lifetimes. The lifetime of a state $|L_J\rangle$ is given by

$$T_{L_J} = \left(\sum_{L'_{J'}} {}^{A}|L_J\rangle \rightarrow |L'_{J'}\rangle \right)^{-1}$$

where the sum is over all states $|L'_{J'}\rangle$ with energy less than that of $|L_J\rangle$. Table 3 compares available measurements of Cs lifetimes with our calculated values; agreement is, again, reasonably good.

3. MAGNETIC DIPOLE TRANSITION RATES

The relativistic contribution to the 6S-7S or 6S-8S M1 transition amplitude is

$$\mathcal{M}_{REL} = e \int g_1 \frac{(kr)}{\omega} (f_i g_f + g_i f_f) dr \tag{8}$$

where $g_1(kr) = \sqrt{\pi/2kr}\ J_{3/2}(kr)$ is a spherical Bessel function, and k and ω are the wave-number and angular frequency of the absorbed photon, respectively. The formula for $nP_{1/2}$-$n'P_{1/2}$ M1 transitions (as in thallium) was derived in I and is identical to Eq. (8) except for sign. We use our DECF radial wave-functions to compute the numerical results

$$\mathcal{M}_{REL}(6S\text{-}7S) = 9.05 \times 10^{-6}\ |\mu_B| \tag{9}$$

$$\mathcal{M}_{REL}(6S\text{-}8S) = 5.68 \times 10^{-6}\ |\mu_B| \tag{10}$$

These results and additional corrections are summarized in Table 4. The "Lamb correction," discussed in I, arises from the interaction between

TABLE 3. Lifetimes of Cs states

State	Measured lifetime (nsec)	Calculated lifetime (nsec)
$6P_{1/2}$	34.0 ± 0.6[a]	26.8
$6P_{3/2}$	29.7 ± 0.2[b]	23.9
$7P_{1/2}$	158 ± 5[c]	149.0
$7P_{3/2}$	135 ± 1[b]	113.0
$8P_{1/2}$	307 ± 14[e]	351.0
$8P_{3/2}$	274 ± 12[e]	270.0
$8S_{1/2}$	87 ± 9[d]	82.0

[a] J. K. Link, J. Opt. Soc. Am. 56, 1195 (1966).

[b] S. Svanberg and S. Rydberg, Z. Phys. 227, 216 (1969).

[c] D. W. Pace and J. B. Atkinson, Can. J. Phys. 53, 937 (1975).

[d] J. Marek, Physics Lett. A, 60A, 190 (1977).

[e] J. Marek and K. Niemax, J. Phys. B: Atom. Molec. Phys. 9, L483 (1976).

valence electron spin and core electron orbits. For $S_{\frac{1}{2}}$-$S_{\frac{1}{2}}$ transitions this is given by:

$$\mathcal{M}_L = -\frac{1}{3} e^2 \langle W \rangle \mu_B \quad . \tag{11}$$

Here $\langle W \rangle = \int_0^\infty F(r_1)[\int_{r_1}^\infty \rho(r_2) r_2 dr_2] F'(r_1) r_1^2 dr_1$ where F, F' are the non-relativistic 6S, 7S(8S) radial wave-functions respectively, and $\rho(r_2)$ is a spherically symmetric core electron density, as in I. The "orbit-orbit" correction vanishes for $S_{\frac{1}{2}}$-$S_{\frac{1}{2}}$ transitions.

The relativistic and "Lamb" contributions to the g-factor anomaly for the $6^2S_{\frac{1}{2}}$ state may be computed in the same way. As previously noted by Perl[9] and by Phillips,[10] the calculation of relativistic effects leads to a g-factor anomaly which is too small and of the wrong sign when compared with experimental results. It has been suggested by a number of authors that interconfiguration interaction[10,4,11] might be responsible for the discrepancy. As discussed in I, electrostatic interaction of the outer electron with excited core states does not by itself affect M1 transition amplitudes or the g-factor anomaly since it mixes only those configurations which have the same total angular momentum and spin ($^2S_{\frac{1}{2}}$). However, in second order, spin orbit coupling allows an admixture of different L-S states (such as $^2P_{\frac{1}{2}}$, $^4P_{\frac{1}{2}}$ in Cs) which can give rise to finite contributions to M1 transitions or g-anomalies. Our detailed calculation of this effect is similar to that presented for thallium in I, and differs only slightly from the work of Phillips.[10] The ground configuration of Cs is $1s^2 \ldots 5p^6 6s$. For first-order excited configurations, we take $1s^2 \ldots 5p^5 6s6p$ or $1s^2 \ldots 5p^5 7s6p$. The outer s and excited p electrons can form ^1P or ^3P states which we label by ψ_1^n, ψ_2^n

respectively (where n corresponds to the nS valence electron). Thus the perturbed 6S, 7S states are written

$$|\bar{6S}\rangle = |6S\rangle + \alpha_1\psi_1^6 + \alpha_2\psi_2^6 + \beta_1\psi_1^7 + \beta_2\psi_2^7 \tag{12}$$

$$|\bar{7S}\rangle = |7S\rangle + \gamma_1\psi_1^6 + \gamma_2\psi_2^6 + \delta_1\psi_1^7 + \delta_2\psi_2^7 \tag{13}$$

L·S coupling mixes the $^2S(^1P)$ states with $^2P(^1P)$ states, and also mixes $^2S(^3P)$ states with $^2P(^3P)$ and $^4P(^3P)$ states. Thus we obtain in second order:

$$\begin{aligned}|\bar{6S}\rangle = {} & |6S\rangle + \ldots + \alpha_1 A_1(^2\phi_1^6) + \alpha_2 A_2(^2\phi_3^6) \\ & + \alpha_2 A_2'(^4\phi_3^6) + \beta_1 B_1(^2\phi_1^7) + \beta_2 B_2(^2\phi_3^7) + \beta_2 B_2'(^4\phi_3^7)\end{aligned} \tag{14}$$

$$\begin{aligned}|\bar{7S}\rangle = {} & |7S\rangle + \ldots + \gamma_1 C_1(^2\phi_1^6) + \gamma_2 C_2(^2\phi_3^6) \\ & + \gamma_2 C_2'(^4\phi_3^6) + \delta_1 D_1(^2\phi_1^7) + \delta_2 D_2(^2\phi_3^7) + \delta_2 D_2'(^4\phi_3^7)\end{aligned} \tag{15}$$

The $^m\phi_\ell^n$ are $^mP(^\ell P)$ states with s-electron radial quantum number n. The A_i, B_i, C_i, D_i, are determined by the electrostatic interaction between outer electrons. The expressions for this interaction are as presented by Phillips except that we find a result $\sqrt{6}$ times larger from anti-symmetrizing initial and final states. For example,

$$A_1 = \frac{\sqrt{6}}{2}\,\frac{F_0 + G_1}{\Delta E} \tag{16}$$

where F_0 and G_1 are the direct and exchange electrostatic integrals and ΔE is the perturbation energy denominator.

The second order coefficients α_i, β_i, γ_i, δ_i are determined by fine structure matrix elements of the 5p electron state, as computed by Phillips. For example, $\alpha_1 = \xi/\sqrt{2}\,\Delta E$, where ξ is the spin-orbit parameter of the

5p-hole. Our value of $\xi/\Delta E = 0.07$ calculated with OECF wave functions differs slightly from Phillips' estimate $\xi/\Delta E \cong 0.10$. The coefficients are evaluated numerically using OECF wave-functions and contribute as follows to the 6S-7S M1 amplitude:

$$\mathcal{M}_{II}(6S\text{-}7S) = (\alpha_1 A_1 \gamma_1 C_1 + \beta_1 B_1 \delta_1 D_1)\left(\frac{g(^2P) - g(^2S)}{2}\right) + (\alpha_2 A_2 \gamma_2 C_2 + \alpha_2 A_2' \gamma_2 C_2' + \beta_2 B_2 \delta_2 D_2 + \beta_2 B_2' \delta_2 D_2')\cdot\left(\frac{g(^4P) - g(^2S)}{2}\right) \tag{17}$$

The results for $\mathcal{M}_{II}(6S\text{-}7S)$ and similar corrections for the 6S-8S M1 amplitude and the 6S g-factor anomaly are presented in Table 4. Similar corrections due to the $(5p^5 6p5d)$ configuration have been calculated; however, these are substantially smaller (~25% of that obtained from Eq. (17)). The overall uncertainty in the interconfiguration interaction correction could be as much as a factor of two or three. However, as can be seen from Table 4, these calculated corrections are too small to account for the observed 6S g-factor and 6S-7S M1 amplitude by an order of magnitude. This discrepancy is not improved much by including contributions of $5p^5 n'pns$ $(n' > 6)$ or $5p^5 n'pnd$ $(n' > 6,\ n > s)$ configurations since their contributions diminish rapidly as n, n' increase. Our conclusion, consistent with that of Phillips, is that the observed anomalies are not due to interconfiguration interaction of this type.

An appreciable correction to the M1 amplitude arises from hyperfine mixing. The size of this effect can be derived from I-59, as modified for Cs $^2S_{\frac{1}{2}}$ states. We find

$$\left(\langle n'S,F|H_{HFS}|6S,F\rangle - \langle 6S,F'|H_{HFS}|nS,F'\rangle\right)\cdot \frac{\langle nS_{\frac{1}{2}},\ F'|M1|nS_{\frac{1}{2}},\ F\rangle}{E_{6S} - E_{nS}} \tag{18}$$

The amplitude vanishes for $F = F'$; this unlike the other amplitudes it only

affects F=3 → F'=4 or F=4 → F'=3 transitions. The hyperfine integrals are evaluated numerically, and we employ:

$$\langle nS_{1/2}F'|M1|nS_{1/2}F\rangle = -\frac{e}{2}\langle F'm_F'|\underset{\sim}{\sigma}|F_I m_F\rangle \qquad (19)$$

The numerical results are summarized in Table 4. An observation of the 3→4 and 4→3 transitions with the same accuracy that Bouchiat and Pottier[12] reported for the 4→4 and 3→3 components of the 6S-7S transitions would clearly reveal the hyperfine correction.

TABLE 4. Summary of contributions to the M1 transition rates.

	$6S_{1/2}$ g-factor ($\delta g/\lvert g\rvert$) anomaly ($g = -2$)	$6S_{1/2}$-$7S_{1/2}$	$6S_{1/2}$-$8S_{1/2}$
Relativistic	$+1.75\times10^{-5}$	$+9.05\times10^{-6}$	$+5.68\times10^{-6}$
Lamb	$+6.2\times10^{-6}$	$+2.87\times10^{-6}$	$+1.78\times10^{-6}$
Interconfiguration Interaction	-8.3×10^{-6}	-7.0×10^{-6}	-5.9×10^{-6}
Hyperfine mixing	--	$8.36\times10^{-6}\times$ (F - F')	$4.02\times10^{-6}\times$ (F - F')
Observed value	$-1.181\pm0.002\times10^{-4}$ [a]	$-4.24\pm0.34\times10^{-5}$ [b]	--

[a] P. A. Vanden Bout, et al., Phys. Rev. 165, 88 (1968).

[b] M. A. Bouchiat and L. Pottier, Jour. de Phys. Lettres 37, L-79 (1976).

The poor agreement indicates that we do not fully understand the small 10^{-4} to 10^{-5}, up to fourth order, effects contributing to the M1 amplitudes. There do not affect the calculation of $\mathcal{E}_{PV}$ since that calculation depends on large, first-order, amplitudes such as $\langle E1\rangle_{SP}$ and $\psi(\vec{r}=0)$. The small size of $\mathcal{E}_{PV}$ is determined only by the small size of G_F.

4. CALCULATION OF PARITY VIOLATING E1 AMPLITUDE

According to the Weinberg-Salam model, the parity violating electron-nucleus interaction provides the following interaction matrix element (I-64):

$$\langle \psi_1 | H_{PV} | \psi_2 \rangle = -\frac{GQ_W}{2\sqrt{2}} \psi_1^*(\vec{x}) \gamma_5 \psi_2(\vec{x}) \Big|_{(\vec{x}=0)} \tag{20}$$

This mixes S-states with opposite parity p-states, as follows:

$$|\overline{nS_{\frac{1}{2}}}\rangle = |nS_{\frac{1}{2}}\rangle + \sum_{W} \frac{\langle n'P_{\frac{1}{2}} | H_{PV} | nS_{\frac{1}{2}} \rangle}{E_{nS} - E_{WP}} |n'P_{\frac{1}{2}}\rangle \tag{21}$$

Thus Eq. (20) can be reduced to:

$$\langle n'P_{\frac{1}{2}} | H_{PV} | nS_{\frac{1}{2}} \rangle = i \frac{GQ_W}{8\sqrt{2\pi}} (f_p g_s - f_s g_p) \Big|_{r=0} \cdot \delta_{m_S m_p} \tag{22}$$

The "r=0" symbol indicates that the expression is averaged over the nuclear volume, and we assumed a constant nucleon density for $r < 0.016$fm. An alternative procedure would be to assume a point-like nucleus and evaluate $\langle H_{PV} \rangle$ at the nuclear radius; this produces a value 2% larger.

An E1 transition amplitude is now possible between the perturbed S-states. Its value is given by

$$\langle \overline{nS_{\frac{1}{2}}} | E1 | \overline{6S_{\frac{1}{2}}} \rangle = \sum_{W} \left\{ \langle nS_{\frac{1}{2}} | E1 | n'P_{\frac{1}{2}} \rangle \frac{\langle n'P_{\frac{1}{2}} | H_{PV} | 6S_{\frac{1}{2}} \rangle}{E_{6S} - E_{n'}} + \frac{\langle nS_{\frac{1}{2}} | H_{PV} | n'P_{\frac{1}{2}} \rangle}{E_{nS} - E_{n'}} \langle n'P_{\frac{1}{2}} | E1 | 6S_{\frac{1}{2}} \rangle \right\} \tag{23}$$

where

$$\langle nS_{\frac{1}{2}} | E1 | n'P_{\frac{1}{2}} \rangle = e \langle nS_{\frac{1}{2}} | \vec{\epsilon} \cdot \vec{r} | n'P_{\frac{1}{2}} \rangle = \frac{e}{3} \int f_S \, r f_r \, dr \tag{24}$$

and the last expression is derived for the particular case $m_S = m_p = -\frac{1}{2}$, $\vec{\epsilon} = \hat{e}_z$. The numerical results are summarized in Table 5, where Eq. (23)

has been evaluated by two methods:

1. A finite sum over the nearest four intermediate p-states
2. The use of the Dirac Green's function.

The Green's function automatically includes all intermediate states, including continuum and auto-ionizing states as shown in I. The two methods give similar results, as shown in Table 5. The Green's function method is considered more accurate, since it is more complete.

In the Weinberg model, with $\sin^2\theta_W = 0.30$ as suggested by the experiment of Reines et al.,[12]

$$Q_W = -\left((4\sin^2\theta_W - 1)Z + N\right) = -99 \tag{25}$$

for Cs^{133}. This leads to a value of $\mathcal{E}_{PV} = -i3.47 \times 10^{-9}|\mu_B|$ for the $6S_{\frac{1}{2}}$-$7S_{\frac{1}{2}}$ transition. This corresponds to a circular polarization (circular dichroism) of:

$$P = \frac{2\mathrm{Im}(\mathcal{E}_{PV})}{\mathcal{M}_{exp}} = 1.64 \times 10^{-4} \tag{26}$$

Bouchiat and Bouchiat,[4] using non-relativistic wave functions with a relativistic correction factor for $\langle H_{PV}\rangle$, a modified Bates-Damgaard method for $e\langle\vec{\epsilon}\cdot\vec{r}\rangle$, and a finite sum over the nearest four P states, obtained a somewhat higher estimate of $-i4.7 \times 10^{-9}\ |\mu_B|$ for $\mathcal{E}_{PV}$ in this transition.

Using our analysis of hyperfine structure and excited states decay rates, we can form a reasonable estimate of errors. Our hyperfine structure and fine structure calculations indicate that the magnitudes of the P-state wave functions as $r \to 0$ are ~10% lower than physically accurate. However, decay rate comparisons indicate that our $\langle E1\rangle$ matrix

TABLE 5A. Calculation of $\mathcal{E}_{PV}$ for the $6S_{\frac{1}{2}}$-$7S_{\frac{1}{2}}$ transition.

Method 1:

Intermediate P-state	$\frac{e}{3}\frac{\langle 7S\|r\|nP_{\frac{1}{2}}\rangle \langle nP_{\frac{1}{2}}\|H_{PV}\|6S\rangle}{E_{6S}-E_n}$	$\frac{e}{3}\frac{\langle 7S\|H_{PV}\|nP_{\frac{1}{2}}\rangle \langle nP_{\frac{1}{2}}\|r\|6S\rangle}{E_{7S}-E_n}$
$\|6P\rangle$	$-i\ 7.823\times10^{-11}\ Q_W\|\mu_B\|$	$+i\ 6.912$
$\|7P\rangle$	$+i\ 5.259$	$-i\ 0.809$
$\|8P\rangle$	$+i\ 0.303$	$-i\ 0.093$
$\|9P\rangle$	$+i\ 0.084$	$-i\ 0.031$
Total	$-i\ 2.18$	$+i\ 5.98$

$$= i\ 3.80\times10^{-11}\ Q_W|\mu_B|$$

Method 2:

$-i\ 1.75$ $\qquad$ $+i\ 5.24$

$$= i\ 3.50\times10^{-11}\ Q_W|\mu_B|$$

TABLE 5B. Calculation of $\mathcal{E}_{PV}$ for the $6S_{1/2} \rightarrow 8S_{1/2}$ transition.

Method 1:

Intermediate P-state	$\frac{e}{3}\frac{\langle 8S\|r\|nP_{1/2}\rangle \langle nP_{1/2}\|H_{PV}\|6S\rangle}{E_{6s} - E_{np}}$	$\frac{e}{3}\frac{\langle 8S\|H_{PV}\|nP_{1/2}\rangle \langle nP_{1/2}\|r\|6S\rangle}{E_{8s} - E_{np}}$
$\|6P\rangle$	$-i\ 1.935 \times 10^{-11}\ Q_W\|\mu_B\|$	$+i\ 2.445$
$\|7P\rangle$	$-i\ 4.751$	$+i\ 0.647$
$\|8P\rangle$	$+i\ 5.027$	$-i\ 0.303$
$\|9P\rangle$	$+i\ 0.366$	$-i\ 0.054$
Total	$-i\ 1.29$	$+i\ 2.74$

$$= i\ 1.44 \times 10^{-11}\ Q_W|\mu_B|$$

Method 2:

$-i\ 0.81$ $\qquad$ $+i\ 2.29$

$$= i\ 1.48 \times 10^{-11}\ Q_W|\mu_B|$$

elements are too large by ~10%. These errors cancel in the evaluation of $\mathcal{E}_{PV}$ and our $\mathcal{E}_{PV}$ error should not be greater than ~10%.

5. CALCULATION OF THE STARK EFFECT E1 TRANSITIONS

In actual experimental technique (see Bouchiat and Pottier) $\mathcal{M}$ and $\mathcal{E}_{PV}$ are measured in interference with the E1 transitions induced by an external electric field. $\mathcal{M}$ and $\mathcal{E}_{PV}$ are not directly observed but are compared to $\mathcal{E}_S$, which is calculated. Therefore, it is important to calculate a reliable value of $\mathcal{E}_S$.

The coordinate system used in the calculation is illustrated in Fig. 2, and is the same used in I. An electric field $E_o\hat{e}_y$ is perpendicular to the photon propagation vector $\hat{e}_x$. The photon has polarization $\vec{\varepsilon} = \cos\theta\hat{e}_y + \sin\theta\hat{e}_z$, and the $^2S_{\frac{1}{2}}$ states are mixed with $P_{\frac{1}{2}}$, $P_{\frac{3}{2}}$ states by Stark effect.

$$|\overline{nS_{\frac{1}{2}}}\rangle = |\overline{nS_{\frac{1}{2}}}\rangle + \sum_{n'P_{\frac{1}{2}}} \langle n'P_{\frac{1}{2}}|\frac{e\vec{E}_o\cdot\vec{r}}{\Delta E_{\frac{1}{2}}}|nS_{\frac{1}{2}}\rangle\ |n'P_{\frac{1}{2}}\rangle + \sum_{n'P_{\frac{3}{2}}} \langle n'P_{\frac{3}{2}}|\frac{e\vec{E}_o\cdot\vec{r}}{\Delta E_{\frac{3}{2}}}|nS_{\frac{1}{2}}\rangle\ |n'P_{\frac{3}{2}}\rangle \tag{27}$$

There is an E1 transition amplitude $\mathcal{E}_S$ between the perturbed states, which we represent as a 2×2 matrix whose rows and columns are labeled by $m_J(6S_{\frac{1}{2}})$ and $m_J(nS_{\frac{1}{2}})$ respectively

$$\mathcal{E}_S = \langle \overline{nS_{\frac{1}{2}}}|e\hat{\vec{\varepsilon}}\cdot\vec{r}|\overline{6S_{\frac{1}{2}}}\rangle$$

$$= e^2E_o \cdot \begin{array}{c|cc} m_J(7S_{\frac{1}{2}}) = & \frac{1}{2} & -\frac{1}{2} \\ \hline \frac{1}{2} & \alpha\cos\theta & -i\beta\sin\theta \\ -\frac{1}{2} & -i\beta\sin\theta & \alpha\cos\theta \end{array} = m_J(6S_{\frac{1}{2}}) \tag{28}$$

$$\alpha = \frac{1}{9}\sum_{n'P_{1/2}} R_{nS,n'P_{1/2}}\, R_{6S,n'P_{1/2}}\left(\frac{1}{E_n - E_{n'P_{1/2}}} + \frac{1}{E_6 - E_{n'P_{1/2}}}\right)$$
$$+ \frac{2}{9}\sum_{n'P_{3/2}} R_{nS,n'P_{3/2}}\, R_{6S,n'P_{3/2}}\left(\frac{1}{E_6 - E_{n'P_{3/2}}} + \frac{1}{E_n - E_{n'P_{3/2}}}\right) \qquad (29)$$

$$\beta = \frac{1}{9}\sum_{n'P_{1/2}} R_{nS,n'P_{1/2}}\, R_{6S,n'P_{1/2}}\left(\frac{1}{E_6 - E_{n'P_{1/2}}} + \frac{1}{E_n - E_{n'P_{1/2}}}\right)$$
$$+ \frac{1}{9}\sum_{n'P_{3/2}} R_{nS,n'P_{3/2}}\, R_{6S,n'P_{3/2}}\left(\frac{1}{E_n - E_{n'P_{3/2}}} + \frac{1}{E_6 - E_{n'P_{3/2}}}\right) \qquad (30)$$

where

$$R_{6S,nP_{1/2}} = \langle 6S_{1/2}|r|n'P_{1/2}\rangle, \qquad E_6 = E(6S_{1/2}) \ , \qquad (31)$$

etc. The quantities α and β have been evaluated by summation over the nearest $P_{1/2}$, $P_{3/2}$ states, and also by use of the Green's function. The results are summarized in Table 6.

Our results can be compared with the calculation of Bouchiat and Bouchiat, which was used in the experimental determination of $\mathcal{M}$ (6S→7S).[5] Their calculation used the E1 oscillator strengths calculated by Stone and signs determined by the Bates-Damgaard method with a sum over the four lowest energy levels. Their value is $e^2\alpha = -1.62\times10^{-5}\ |\mu_B|/\frac{V}{cm}$ and $|\alpha/\beta| \cong 7.0$ for δ_S(7S-6S). Our value of $|\alpha/\beta|$ is 10.1 and agrees more closely with the experimental result 8.8 ± 0.4. However, our analysis of excited state lifetimes leads us to suspect that our value $e^2\alpha = -1.97\times10^{-5}\ |\mu_B|/\frac{V}{cm}$ is ~10% to 20% too large, so the true

value of $e^2\alpha$ is probably somewhere between our result and that of Bouchiat and Bouchiat.

In Table 7 we combine the calculations of $\mathcal{E}_S$, $\mathcal{M}$, and $\mathcal{E}_{PV}$ in a single 2×2 matrix so that the interference among these amplitudes can be readily extracted. Table 7 gives the (6S→nS) transition amplitudes with the photon directed along $\hat{e}_x$ with polarization $\vec{\varepsilon} = \vec{e}_y\cos\theta + \vec{e}_z\sin\theta$.

TABLE 6. Stark effect E1 amplitudes.

A. $\langle \overline{7S} \vert E1 \vert \overline{6S} \rangle$	$e^2\alpha \left(\frac{\vert\mu_B\vert}{volts/cm}\right)$	$e^2\beta \left(\frac{\vert\mu_B\vert}{volts \cdot cm}\right)$	$\left\vert\frac{\alpha}{\beta}\right\vert$
Finite sum method:	-2.043×10^{-5}	-1.78×10^{-6}	11.5
Green's function:	-1.972×10^{-5}	-1.96×10^{-6}	10.06
Experimental value:	--	--	8.8 ± 0.4
B. $\langle \overline{8S} \vert E1 \vert \overline{6S} \rangle$			
Finite sum method:	-3.132×10^{-5}	-3.71×10^{-6}	8.45
Green's function:	-3.166×10^{-5}	-3.97×10^{-6}	7.86

TABLE 7

$n^2S_{1/2} - 6^2S_{1/2}$ Transition amplitudes.

$\langle \overline{nS} | E1 + M1 + \varepsilon_S | \overline{6S} \rangle =$

		$+\frac{1}{2}$	$-\frac{1}{2} = m_z(6^2S_{1/2})$
m_z $(nS_{1/2})$	$= +\frac{1}{2}$	$\alpha' \cos\theta$ $+ \mathcal{M} \cos\theta$ $- \delta_{PV} \sin\theta$	$-i\,\beta' \sin\theta$ $+i\mathcal{M} \sin\theta$ $+i\,\delta_{PV} \cos\theta$
	$= -\frac{1}{2}$	$-i\,\beta' \sin\theta$ $-i\mathcal{M} \sin\theta$ $-i\,\delta_{PV} \cos\theta$	$\alpha' \cos\theta$ $- \mathcal{M} \cos\theta$ $+\delta_{PV} \sin\theta$

$$\vec{\varepsilon} = \hat{e}_y \cos\theta + \hat{e}_z \sin\theta$$

$$\alpha' = e^2\alpha\, E_y$$

$$\beta' = z\, e^2\beta\, E_z$$

CHAPTER II REFERENCES

*This research is supported by the U.S. Energy Research and Development Administration.

1. D. V. Neuffer and E. D. Commins, LBL-6043, submitted to Phys. Rev. A.
2. T. Tietz, J. Chem. Phys. 22, 2094 (1954).
3. S. Weinberg, Phys. Rev. Lett. 19, 1264 (1967);
   A. Salam, in Elementary Particle Theory, ed. N. Svartholm (Alquist and Vorlag, Stockholm, 1968).
4. M. A. Bouchiat and C. Bouchiat, Phys. Lett. 48B, 111 (1974), Jour. de Phys. 35, 899 (1974), Jour. de Phys. 36, 493 (1975).
5. M. A. Bouchiat and L. Pottier, Jour. de Phys. Lett. 37, L-79 (1976).
6. C. E. Moore, Atomic Energy Levels, Vol. III, Circular of Nat. Bureau of Standards 467 (1958).
7. M. E. Rose, Relativistic Electron Theory, (J. Wiley and Sons, New York, 1961).
8. C. M. Lederer, J. M. Hollander, and I. Perlman, Table of Isotopes (J. Wiley and Sons, New York, 1967).
9. W. Perl, Phys. Rev. 91, 852 (1953).
10. M. Phillips, Phys. Rev. 88, 202 (1952).
11. I. B. Khriplovich, Sov. J. Nucl. Phys. 21, 538 (1975); (Yad. Fiz. 21, 1946).
12. F. Reines et al., Phys. Rev. Lett. 37, 315 (1976).